Tectonics®

RESEARCH ARTICLE
10.1029/2025TC009243

Key Points:

- The first arrival of the East Anatolian-derived detritus along the northern Arabian margin occurred during the late Campanian
- Initial docking of the Arabian Plate and Eastern Anatolia dates back to the late Campanian
- Contrary to previous models, the southern branch of the Neo-Tethys Ocean closed before the northern branch

Supporting Information:

Supporting Information may be found in the online version of this article.

Correspondence to:

R. Akdoğan and X. Hu,
rakdogan@itu.edu.tr;
remziyeak@gmail.com;
huxm@nju.edu.cn

Citation:

Akdoğan, R., Hu, X., Topuz, G., Hakyemez, A., Catanzariti, R., Ma, A., et al. (2026). Late Campanian (74–71 Ma) Arabia–Eastern Anatolia collision and its geodynamic implications. *Tectonics*, *45*, e2025TC009243. https://doi.org/10.1029/2025TC009243

Received 20 OCT 2025
Accepted 22 JUN 2026

Author Contributions:

Conceptualization: Remziye Akdoğan, Xiumian Hu, Gültekin Topuz
Data curation: Remziye Akdoğan, Aynur Hakyemez, Rita Catanzariti
Formal analysis: Remziye Akdoğan, Aynur Hakyemez, Rita Catanzariti, Anlin Ma
Funding acquisition: Remziye Akdoğan, Xiumian Hu
Investigation: Remziye Akdoğan
Methodology: Remziye Akdoğan
Project administration: Remziye Akdoğan, Xiumian Hu
Resources: Remziye Akdoğan

Late Campanian (74–71 Ma) Arabia–Eastern Anatolia Collision and Its Geodynamic Implications

Remziye Akdoğan[1,2], Xiumian Hu[1], Gültekin Topuz[2,3], Aynur Hakyemez[4], Rita Catanzariti[5], Anlin Ma[1], Yalçın E. Ersoy[3], and İbrahim Uysal[6]

[1]State Key Laboratory of Critical Earth Material Cycling and Mineral Deposits, School of Earth Sciences and Engineering, Nanjing University, Nanjing, China, [2]Istanbul Technical University, Eurasia Institute of Earth Sciences, Istanbul, Türkiye, [3]Department of Geological Engineering, Dokuz Eylül University, İzmir, Türkiye, [4]Department of Geological Research, General Directorate of Mineral Research and Exploration, Ankara, Türkiye, [5]Istituto di Geoscienze e Georisorse (IGG), Consiglio Nazionale delle Ricerche, Pisa, Italy, [6]Department of Geological Engineering, Karadeniz Technical University, Trabzon, Türkiye

Abstract The East Anatolian Plateau is a major collisional feature within the Tethyan realm formed as a late-stage result of the collision between East Anatolia and the Arabian Platform. The timing of this collision is highly debated, with estimates from the Late Cretaceous to the Miocene. This study presents new biostratigraphic and detrital zircon U–Pb–Hf data from upper Campanian and Danian siliciclastic rocks of the Arabian Foreland Basin, ~40 km south of the Bitlis Suture. Upper Campanian rocks contain a dominant zircon age cluster (100–83 Ma) with εHf(t) values ranging from −7 to +6, whereas overlying Danian sandstones yield broader age spectra with clusters at 100–65 Ma, 750–500 Ma, and 1,100–800 Ma. The absence of Late Cretaceous magmatism on the Arabian Plate indicates derivation from the magmatic arc north of the Bitlis Suture. The late Campanian–Danian provenance shift likely reflects erosion of the upper arc and exhumation of metamorphic massifs representing middle- to lower-crustal levels of the magmatic arc and the subducted Arabian margin, indicating that the Arabia–Eastern Anatolia collision began in the late Campanian (~74–71 Ma). Reassessment of published detrital zircon data from the Iranian foreland suggests later collision along the Zagros Suture (Maastrichtian-early Paleocene in the Kermanshah and Khorramabad areas). Final Eurasia–Arabia suturing occurred along the İzmir–Ankara–Erzincan and Zagros sutures, linked across West Azerbaijan (Iran), providing a coherent explanation for the pronounced Mesozoic–early Cenozoic geological contrasts between Eastern Anatolia and NW Iran.

1. Introduction

The Alpine–Himalayan orogenic system is one of the world's longest active collisional belts, extending over 15,000 km from Spain to Indonesia. Its evolution is linked to the closure of the Tethys Ocean and its various branches (e.g., Metcalfe, 2013; Yin, 2006; Şengör, 1991). Türkiye and Iran are located on this orogenic belt, and are made up of several continental blocks separated by sutures representing the traces of the different branches of the Tethys Ocean (Figure 1; Okay & Tüysüz, 1999; Şengör & Yilmaz, 1981). The İzmir–Ankara–Erzincan Suture (IAES) marks the northern branch of the Neo-Tethys, and the Bitlis–Zagros Suture the southern branch. Closure of the northern branch, the northern Neo-Tethys, is thought to have occurred during the Paleocene-early Eocene, as the middle Eocene volcaniclastic rocks seal the suture zone (Okay et al., 2022; Okay & Tüysüz, 1999; Topuz et al., 2011). The southern branch, the southern Neo-Tethys, is delineated by the >1,500 km long Bitlis–Zagros Suture, with its western segment referred to as the Bitlis Suture. This suture zone extends from the Eastern Mediterranean Sea in the west to the Oman Sea in the east, where active subduction is still ongoing (Figure 1; for reasons of legibility and brevity, the Oman Sea is kept outside the map area). This oceanic domain likely opened in the Late Triassic during the rifting of the Anatolide–Tauride Block from the northern margin of Gondwana (Robertson et al., 2012; Şengör & Yilmaz, 1981). While the initiation of convergence between the Anatolide–Tauride Block and the Arabian Plate is well constrained by the formation ages of supra-subduction zone ophiolites, such as Kızıldağ, Troodos, Kermanshah, and Oman (U–Pb zircon: 96–92 Ma; Dilek & Thy, 2009; Bingöl et al., 2018), the timing of complete consumption of oceanic lithosphere and the onset of the continental collision remains debated. Estimates vary widely, from the Late Cretaceous to the Pliocene (Table 1; e.g., Alavi, 1994; Agard et al., 2011; Ballato et al., 2011; Berberian & King, 1981; Darin & Umhoefer, 2022;

Supervision: Xiumian Hu
Validation: Remziye Akdoğan, Xiumian Hu, Gültekin Topuz
Visualization: Remziye Akdoğan
Writing – original draft: Remziye Akdoğan, Xiumian Hu, Gültekin Topuz, Aynur Hakyemez, Rita Catanzariti, Anlin Ma, Yalçın E. Ersoy, İbrahim Uysal
Writing – review & editing: Remziye Akdoğan, Xiumian Hu, Gültekin Topuz, Aynur Hakyemez, Rita Catanzariti, Anlin Ma, Yalçın E. Ersoy, İbrahim Uysal

Hempton, 1985; Mouthereau et al., 2012; Okay et al., 2010; Şengör & Yilmaz, 1981; Sun et al., 2023; van Hinsbergen et al., 2020, 2024; Yazgan, 1984; Yazgan & Chessex, 1991; Yılmaz, 1993).

These discrepancies in the timing of the continental collision led to contrasting tectonic models that propose either one or two subduction zones, involving intraoceanic arc accretion and final continental collision, and suggest both synchronous and diachronous collision scenarios. The paleogeographic role of the Late Cretaceous metamorphic belt situated between the Arabian Plate and the Anatolide–Tauride Block, the Bitlis–Pütürge Massif (Figure 2), remains a key point of debate among the proposed tectonic models. The massif comprises Late Cretaceous greenschist-to amphibolite-facies continental rock assemblages, with locally preserved kyanite-bearing eclogite and blueschist assemblages (Oberhänsli et al., 2010, 2013; Okay et al., 1985). Competing models interpret it as (a) an independent continental block bounded by two subduction zones (e.g., Oberhänsli et al., 2010, 2013; Robertson et al., 2012; Şengör et al., 2008), (b) an eastern promontory of the Anatolide–Tauride Block (van Hinsbergen et al., 2020) or (c) the northern subducted edge of the Arabian Plate, with the suture located north of the massif (e.g., Yazgan, 1984). These alternative interpretations imply different geometries and timings for the final stages of Neo-Tethyan closure. Overall, it is accepted that the northern Neo-Tethys closed earlier than the southern one (e.g., Okay et al., 2010, 2020a; Robertson & Dixon, 1984; Robertson et al., 2012; Şengör, 1991; Şengör & Yilmaz, 1981). Thus, the closure of the southern Neo-Tethys is also referred to as the collision between the Arabian Platform and Eurasia. Precisely constraining the closure timing of both branches is therefore critical for reconstructing the geological evolution of Eastern Anatolia and the NW Iranian Block, as well as for understanding the mechanisms driving plateau formation, widespread Neogene–Quaternary volcanism, and the coupled processes of crustal thickening and lithospheric thinning in the East Anatolian Plateau.

Continental collision occurs when the intervening oceanic lithosphere between two continental domains is entirely subducted, and the opposing continental margins are brought into direct contact (e.g., Hu et al., 2015; Wang et al., 2025, and references therein). The timing of this event can be constrained using multiple geological constraints (see Hu et al., 2016, 2017), including: the transition from passive margin sedimentation to foreland basin deposition; the onset of (ultra)high-pressure ((U)HP) metamorphism in the leading edge of the subducted passive continental margin; molasse deposition; convergence of palaeolatitudes between the two continental margins; similarities or differences in faunal and floral assemblages; compositional and isotopic changes in magmatism reflecting the transition from oceanic to continental subduction; and the development of fold-and-thrust belts in the subducting plate, along with crustal thickening and surface uplift in the overriding continental arc. However, complications arise in the presence of intervening intraoceanic arcs and dual subduction systems within a single oceanic domain. A striking example is provided by the Makran region, where the emplacement of the Oman ophiolite onto the passive continental margin of the Arabian Plate and the onset of continental subduction occurred during the Late Cretaceous. In contrast, subduction and accretion along a separate subduction zone in the Gulf of Oman have persisted from the Early Cretaceous (120–100 Ma) to the present day, without subsequent continental collision (Burg, 2018, and references therein). This highlights that the timing of ophiolite obduction and continental subduction does not necessarily coincide with the timing of initial continental collision. In this context, the distance between the intra-oceanic subduction zone and the active continental margin is critically important. In cases involving an intervening intraoceanic arc, both its formation age range and accretionary history must also be considered when constraining the timing of continental collision.

A robust and direct estimate of the timing of continental collision can be obtained by dating the first arrival of active margin-derived detritus onto the passive continental margin (e.g., Akdoğan et al., 2021; Garzanti, 2019; Hu et al., 2015; Sun et al., 2023; Wang et al., 2025). Moreover, the combined Hf isotopic compositions and trace element signatures of the detrital zircons offer critical clues to their provenance, enabling differentiation between juvenile igneous sources, crustally contaminated magmas, and tectonic environments such as magmatic arcs, intraoceanic arcs, mid-ocean ridges, and oceanic islands. Here we integrate petrographic, biostratigraphic, U–Pb detrital zircon age and Lu–Hf isotopic data from Upper Cretaceous to early Paleocene sandstones of the Arabian Foreland Basin, located ~30–40 km south of the Bitlis Suture (Figure 1). Combined with the constraints from regional geology, sedimentation, and metamorphism, these data show that active-margin detritus first reached the passive-margin basin as early as the late Campanian (~74–71 Ma, Late Cretaceous), thus predating earlier estimates for continental collision. We reevaluated the U–Pb–Hf data on detrital zircons from the literature on sedimentary rocks from the Arabian Foreland Basin in the Iranian segment to compare the timing of the collision with that in SE Anatolia. Finally, we discuss the geodynamic implications of the continental collision during the late Campanian for the geological evolution of eastern Anatolia and NW Iran.

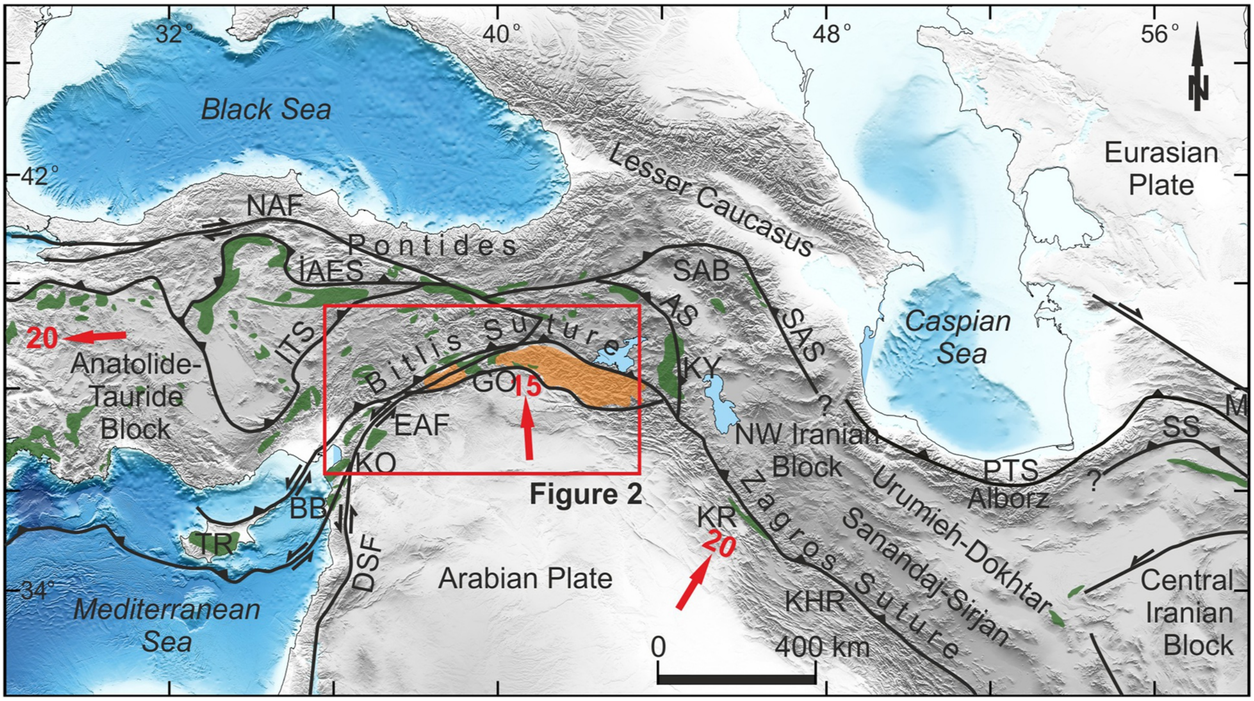

Figure 1. Simplified map showing the main Paleo- and Neo-Tethyan sutures in Türkiye and Iran. Bathymetric and topographic data are sourced from GEBCO (2019). Only well-established sutures and major structural elements are shown; the termination and potential linkage of the Sevan–Akera Suture (SAS) with the Sebzevar Suture (SS) and other sutures remain debated and are therefore not depicted. GPS-derived velocities (mm/yr) of the Arabian Plate relative to Eurasia, after Reilinger et al. (2006), are indicated in red. The Bitlis-Pütürge Massif is highlighted in orange, and ophiolitic units are shown in green. Abbreviations: IAES, İzmir–Ankara–Erzincan Suture; ITS, Inner Tauride Suture; EAF, East Anatolian Fault; NAF, North Anatolian Fault; DSF, Dead Sea Fault; SAS, Sevan-Akera Suture; AS, Azerbaijan Suture; SS, Sebzevar Suture; PTS, Paleo-Tethyan Suture. TR, Troodos Ophiolite; KO, Kızıldağ Ophiolite; BB, Baer–Bassit Ophiolite; GO, Guleman Ophiolite; KY, Khoy Ophiolite; KR, Kermanshah Ophiolite; KHR, Khorramabad; SAB, South Armenian Block; M, Mashhad.

2. Geological Framework

The East Anatolian Plateau is characterized by an average elevation of ca. 2,000 m above sea level, a crustal thickness of 40–58 km, and present-day convergence rates of around 20 mm/yr (e.g., Eken et al., 2021; Reilinger et al., 2006; Zor et al., 2003; Şengör et al., 2003, 2008). Despite the presence of a thickened crust, the lithosphere beneath the plateau is unusually thin (70–80 km), implying that the high elevation is supported by asthenosphere (Şengör et al., 2003). The plateau surface is largely covered by Neogene and Quaternary volcanic and sedimentary rocks. Local exposures of Late Cretaceous high-temperature, medium- to low-pressure metamorphic rocks, together with established premetamorphic stratigraphy, indicate that the East Anatolian Plateau represents the eastward continuation of the Anatolide–Tauride Block (Topuz et al., 2017; Yılmaz et al., 2023). To the east, the plateau is bounded from the northwestern Iranian Block by a roughly north–south–trending Neo-Tethyan Suture, here termed the Azerbaijan Suture, after West Azerbaijan Province of Iran. This suture is marked by Late Cretaceous ophiolites (e.g., Khoy) and associated accretionary complexes (Topuz et al., 2017; Şengör, 1990) and by a prominent positive gravity anomaly marking the paleo-subduction channel (Braitenberg et al., 2025). Alternatively, some studies interpret these ophiolitic rocks as remnants of an ophiolite sheet derived from the northern branch of the Neo-Tethys (e.g., Rolland et al., 2020). In the following section, we outline the stratigraphic framework of the Arabian passive margin, the eastern Anatolide–Tauride Block, and the lithological units that make up the Bitlis Suture.

2.1. The Arabian Foreland

The Arabian passive margin in southeastern Türkiye is underlain by a late Neoproterozoic to early Cambrian crystalline basement and by Precambrian to Paleozoic sedimentary successions (Figure 2; Yılmaz, 1993; Ustaömer et al., 2012; Gürsu et al., 2015). The pre-orogenic Paleozoic–Mesozoic rock associations are mainly dominated by passive-margin carbonate sequences. During the mid-to late Campanian, sedimentation in the

10.1029/2025TC009243

Table 1
Summary of Previous Estimates for the Timing of Continental Collision Along the Bitlis–Zagros Suture

Reference	Region	Timing of the collision	Reasoning	Methods
Berberian and King (1981)	Iran region	Late Cretaceous–Paleocene	Earliest continental collision proposal (~Late Cretaceous) based on stratigraphy, magmatic arcs, ophiolite belts	Stratigraphic correlation
Şengör & Yılmaz (1981)	Iran & the Anatolian regions	Early-Middle Miocene	Closure of the marginal seas	Stratigraphic correlation
Yazgan and Chessex (1991)	Southeastern Anatolia	late Campanian-early Maastrichtian	Orogenic belt growth evidenced by magmatism, metamorphism, ophiolite emplacement and sedimentation	Stratigraphic correlation and geochemistry
Yılmaz (1993)	Southeastern Anatolia	Early Miocene	Regional synthesis	Stratigraphic correlation
Faccenna et al. (2006)	Anatolia	35–30 Ma (latest Eocene to Oligocene)	Change of degree of plate motion and activation of the Afar plume in an extensional setting	Kinematic analysis
Hüsing et al. (2009)	Southeastern Anatolia	ca. 11 Ma (Late Miocene)	Age of the youngest flysch deposit	biostratigraphy
Kaymakci et al. (2010)	Southeastern Anatolia	ca. 11 Ma (Late Miocene)	North–south-directed compression	Kinematic analysis
Okay et al. (2010)	Southeastern Anatolia	ca. 20 Ma (Early Miocene)	Early Miocene exhumation in the Bitlis Massif	Apatite fission-track age data
Agard et al. (2011)	Zagros Mountains, Iran	35-30 Ma (latest Eocene to Oligocene)	Subduction-to-collision transition	synthesis of regional geological features and seismic tomography
Ballato et al. (2011)	Alborz Mountains, Iran	by ca. 36 Ma (late Eocene) soft collision and by ca. 20 Ma (Early Miocene)	Transition from an extensional to a contractional tectonic regime at the late Eocene-early Oligocene	Stratigraphy and provenance
Rolland et al. (2012)	Southeastern Anatolia & Armenia	ca. 48 Ma (early Eocene)	Bitlis HP/LT (blueschists) rock exhumation from a shear zone	40Ar/39Ar muscovite age data
Robertson et al. (2012)	Southeastern Anatolia	Middle Miocene	Volcanic rocks (Helete) are assumed to be Eocene arc volcanic rocks	Regional geology and geochemistry
McQuarrie and van Hinsbergen (2013)	Zagros Mountains, Iran	ca. 27 Ma (late Oligocene)	Shortening estimates	Structural reconstruction
Açlan and Altun (2018)	Southeastern Anatolia	ca. 22 Ma (Aquitanian, Early Miocene)	Early Miocene syn-collisional I-type calc-alkaline magmatism	Geochemistry and geochronology of intrusive rocks
Cavazza et al. (2018)	Southeastern Anatolia	Middle Miocene	Post-collisional cooling and exhumation driven by crustal thickening and strike-slip faulting along the Bitlis Suture	Apatite fission-track and zircon (U-Th)/He age data
Darin et al. (2018)	Southeastern Anatolia	ca. 45 Ma (middle Eocene) soft collision, and ca. 20 Ma (Early Miocene) hard collision	Time of exhumation and magmatic lull between 40 and 20 Ma	Apatite fission-track ages
Su and Zhou (2020)	Zagros Mountains, Iran	Middle Miocene	Crustal shortening after 20 Ma	Restoration of crustal-scale cross-sections
Darin and Umhoefer (2022)	Zagros Mountains, Iran	ca. 45 Ma (middle Eocene) in Eastern Anatolia and by ~20 Ma (Early Miocene) in Zagros	Collision initiated earlier in the Bitlis region than in the Zagros, likely due to irregular continental margins and oblique convergence	Apatite/zircon fission-track age data, stratigraphic analysis and paleostress reconstructions
Topak (2022)	Southeastern Anatolia	Middle Miocene	Northerly sources	Provenance
Sun et al. (2023)	Zagros Mountains, Iran	pre-Eocene collision	Provenance change	Provenance

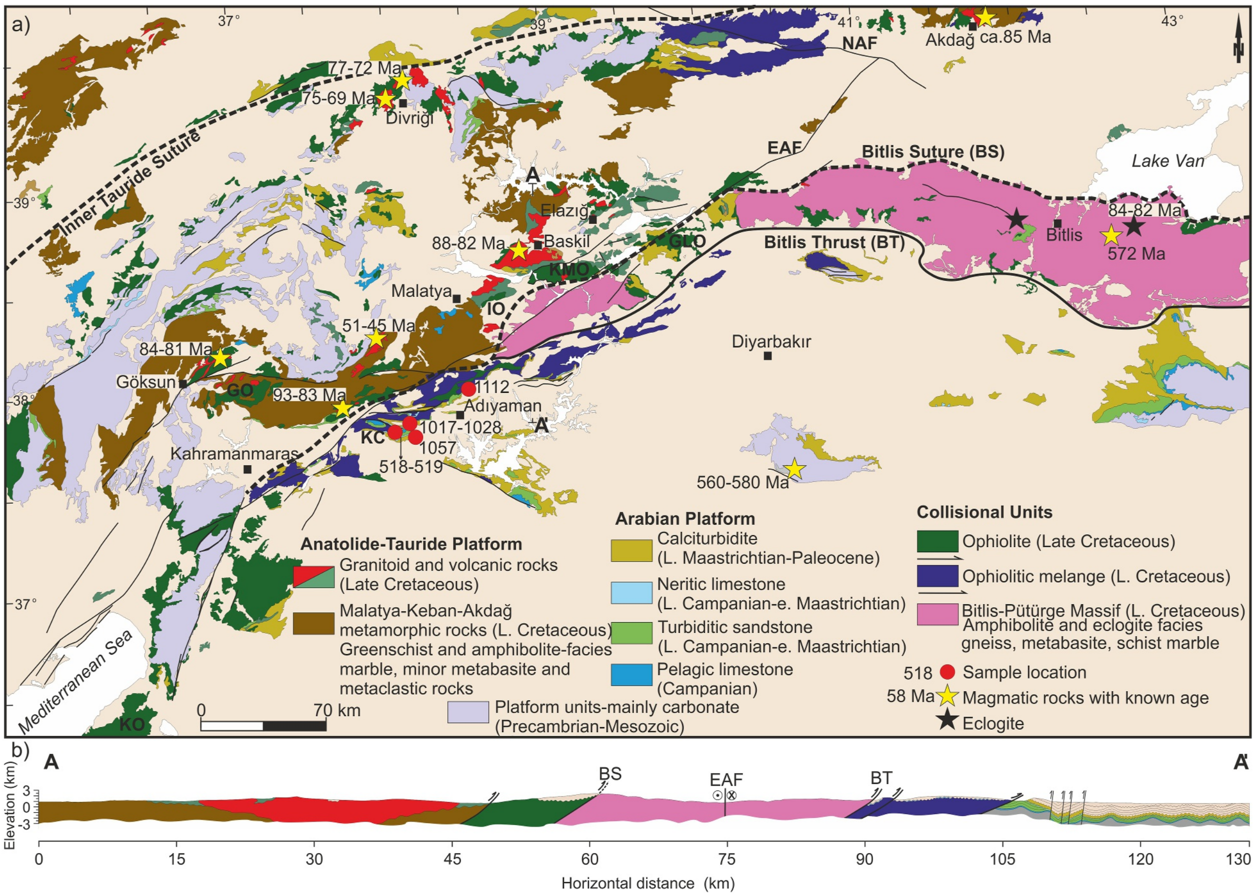

Figure 2. (a) Geological map of southeastern Anatolia near the Bitlis Suture (modified after Konak et al., 2015); (b) Cross section across the Bitlis Suture Zone. Yellow- and black-filled stars indicate previously published U–Pb zircon ages of igneous rocks and eclogites, respectively (see text for references). Red-filled circles denote the samples analyzed. KO, Kızıldağ Ophiolite; GO, Göksun Ophiolite; IO, Ispendere Ophiolite; KMO, Kömürhan Ophiolite; GLO, Guleman Ophiolite; KC, Koçali Complex; BS, Bitlis Suture; NAF, North Anatolian Fault; EAF, East Anatolian Fault; BT, Bitlis Thrust.

region shifted from lagoonal and neritic carbonates to pelagic carbonates, which are overlain by the siliciclastic deposits of the Kastel Formation (Yılmaz et al., 2018). This succession records the transition from passive-margin sedimentation to foreland-basin deposition. The stratigraphic change coincides with the obduction of supra-subduction zone ophiolites and associated mélanges onto the Arabian Platform (Figure 3; Robertson et al., 2016), likely reflecting the transient isostatic effect of ophiolite loading, a mechanism similarly proposed by Şengör and Yilmaz (1981) for the northern margin of the Anatolide–Tauride Block. The late Campanian Kastel Formation, the earliest clastic unit of the Arabian Foreland Basin (Figures 4a and 4b), varies in thickness from 80 to 800 m (Perinçek et al., 1991) and is laterally equivalent to the Amiran Formation in Iran (Homke et al., 2009; Robertson et al., 2016; this study). The Kastel Formation is overlain by the early Maastrichtian Terbüzek Formation, comprising 20–200 m of floodplain deposits, and by the rudist-bearing carbonate succession of the Besni Formation (15–150 m thick), which rests unconformably on underlying units and is capped by a hardground surface (Figures 4c–4f). The Besni Formation is biostratigraphically dated to the late Campanian to early Maastrichtian (Özer, 2025; Robertson et al., 2016; Steuber et al., 2009). $^{87}Sr/^{86}Sr$ isotopic compositions of rudist bivalves correspond to ages of 70–73 Ma (Steuber & Schlüter, 2012; latest Campanian-early Maastrichtian, after Cohen et al., 2025).

The upward shallowing in the Kastel Formation and subsequent subaerial emergence, followed by deposition of Maastrichtian reefal limestone, can be tentatively attributed to detachment of the obducted ophiolite from its oceanic lithosphere and the attainment of a steady-state equilibrium after ophiolite obduction. Although complicated by higher-frequency oscillations, the latest Cretaceous-early Paleocene is characterized by a prominent long-term sea-level fall (ca. 50 m from 77 to 62 Ma; Haq, 2014). The overlying late

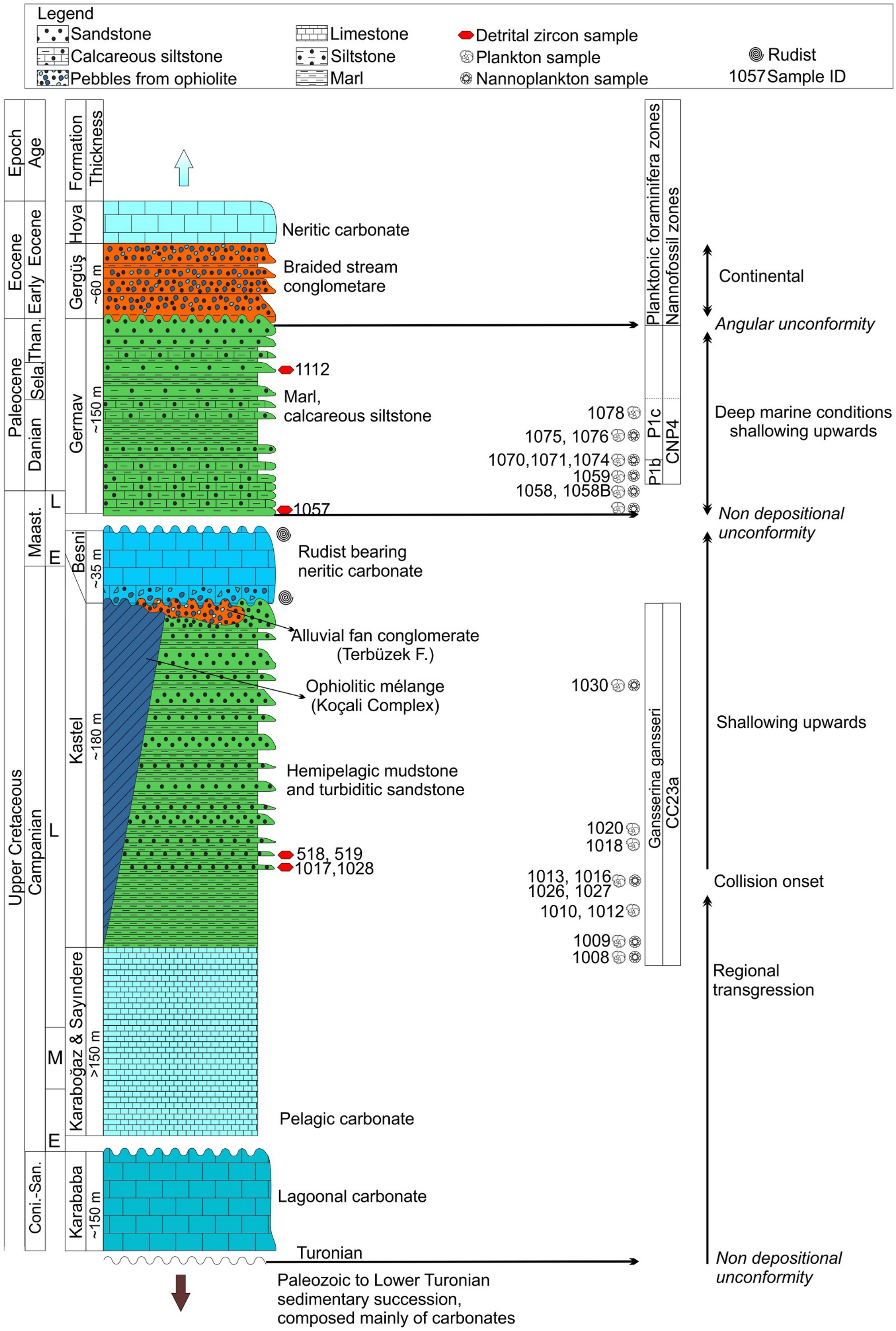

Figure 3. Generalized Late Cretaceous-early Eocene stratigraphic chart of the Arabian Foreland in the study area. Stratigraphy of the Coniacian-Santonian limestones is taken from Yılmaz et al. (2018). For the Eocene and post-Eocene successions on the Arabian Foreland, readers are referred to Duran et al. (1988), Okay et al. (2010), and Robertson et al. (2016 and references therein).

10.1029/2025TC009243

Figure 4. Field photographs from outcrops of the Arabian Foreland Basin in the Adıyaman region. (a) General view of the upper Campanian to Eocene foreland succession; (b) turbidites of the Kastel Formation exposed in the Besni Basin; (c) overlying flood deposits of the Terbüzek Formation; (d) contact between the Terbüzek Formation and the Lower Maastrichtian rudist-bearing shallow-marine carbonates of the Besni Formation; (e) erosional contact between the ophiolitic mélange (Koçali Complex) and Besni Formation; (f) unconformable contact between the Besni Formation and calciturbidites of the Germav Formation.

Maastrichtian–Danian Germav Formation begins with marl-rich calcareous siltstone, passing upward into coarser lenticular sandstones (Figure 4f). This unit is unconformably overlain by the lower Eocene continental red clastics, which grade upward into lower–upper Eocene neritic carbonates. A subsequent regression occurred during the Oligocene, corresponding to a renewed interval of eustatic sea-level lowstand (Miller et al., 2020), and Oligocene strata are notably absent across much of SE Anatolia (Okay et al., 2010; Perinçek et al., 1991). A subsequent marine transgression in the Early Miocene led to the deposition of reefal carbonates, which grade upward into siliciclastic marine turbidites (Duran et al., 1988; Okay et al., 2010). The deposition of these turbidites was contemporaneous with apatite fission-track ages from the Bitlis Massif, implying that they were deposited in front of the Bitlis Thrust and were formerly ascribed to the continental collision between the Arabian Platform and Eastern Anatolia (Okay et al., 2010). During the Middle Miocene, southeastern Anatolia was uplifted above sea level. The stratigraphic succession is capped by Upper Miocene–Pliocene continental clastic and evaporitic deposits. For brevity, post-Eocene units are not distinguished in Figures 2 and 3. For the discussion of Eocene and post-Eocene successions, readers are referred to Duran et al. (1988), Okay et al. (2010), and Robertson et al. (2016 and references therein).

2.2. Eastern Anatolia

Eastern Anatolia, representing the eastern segment of the Anatolide–Tauride Block, comprises two principal lithological associations: (a) Paleozoic to late Mesozoic platform-type carbonate successions with subordinate

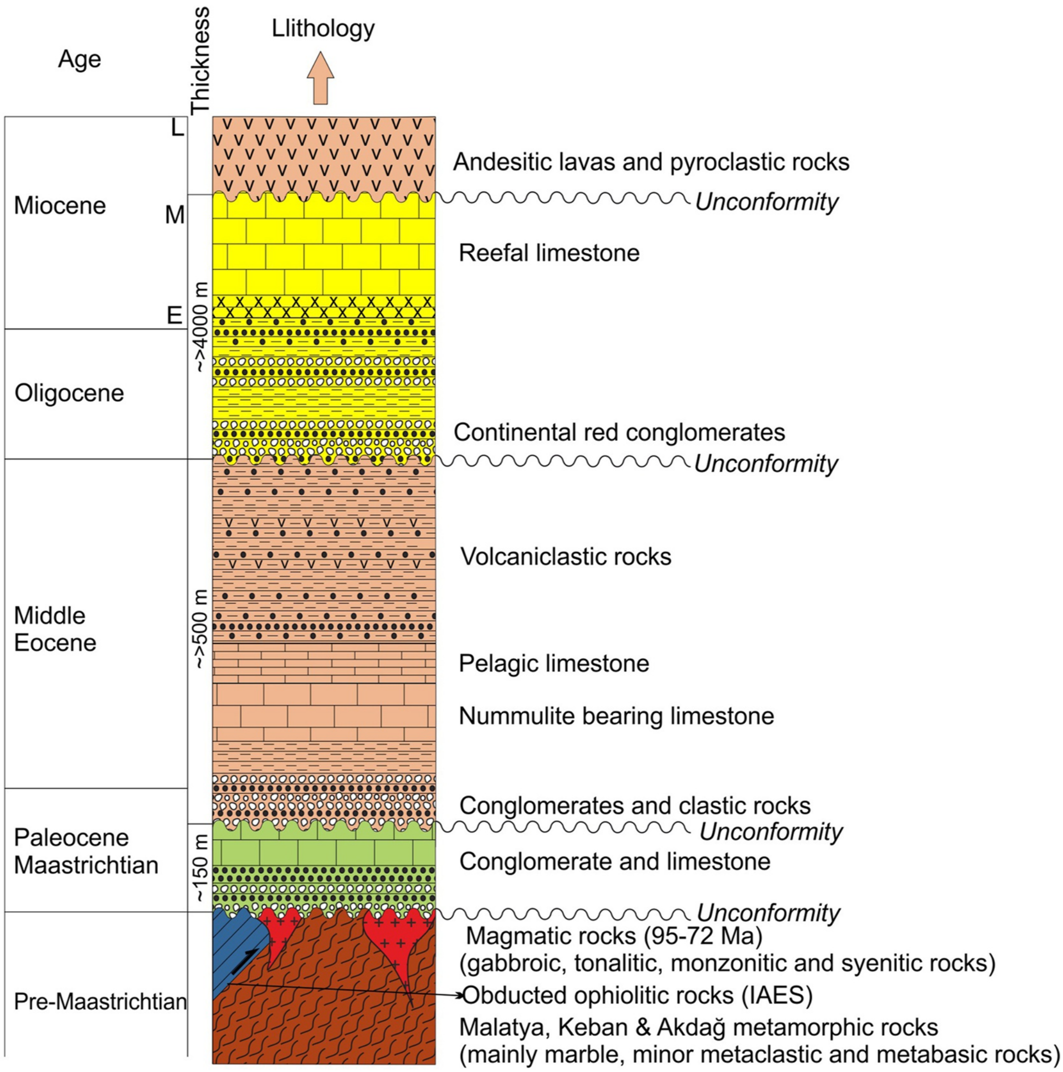

Figure 5. Generalized stratigraphy of Eastern Anatolia (Anatolide-Tauride Block). It is based on the studies of Özcan et al. (2010), Robertson et al. (2016, 2021), Topuz et al. (2017), and Yılmaz et al. (2023).

clastic deposits and minor anorogenic igneous rocks (e.g., Özgül & Turşucu, 1984), and (b) Late Cretaceous greenschist-to amphibolite-facies, high-temperature/low-pressure (HT–LP) metamorphic rocks (Figure 5; Topuz et al., 2017; Rolland et al., 2012). The metamorphic associations, commonly referred to as the Binboğa, Malatya, Keban, and Akdağ metamorphic complexes (Figure 2), are dominated by marbles, with subordinate metaclastic and metabasic lithologies and minor metabauxite. Local occurrences of metasyenitic to metagranitic rocks yield igneous crystallization ages of 430–440 Ma (Topuz et al., 2021). U–Pb zircon and titanite dating constrain the timing of HT–M to LP metamorphism in the Akdağ area to 83 ± 2 Ma and 80 ± 3 Ma (Rolland et al., 2012; Topuz et al., 2017).

The HT–M to LP metamorphic units are crosscut by coeval basic to acidic intrusions with tholeiitic and high-K calc-alkaline to shoshonitic affinity (Beyarslan & Bingöl, 2018; Liu et al., 2022; Rolland et al., 2020; Topuz et al., 2017). They are mainly exposed in the Baskil, Akdağ, and Göksun areas and are collectively referred to in this study as the "Baskil magmatic arc" (Figure 2). U–Pb zircon ages of these igneous rocks range from 88 to 69 Ma (e.g., Ersoy et al., 2024; Ertürk et al., 2022; Eyüboğlu et al., 2019; Karaoğlan et al., 2016; Liu et al., 2022; Rızaoğlu et al., 2006; Sar et al., 2019; Ural et al., 2021). The igneous rocks with crystallization ages of 77 to 69 Ma, mainly exposed in Divriği area, are characterized by shoshonitic and nepheline-normative affinities. The Late Cretaceous HT–LP metamorphism and associated intrusions are interpreted as the mid-to low-crustal section of the continental magmatic arc (Karaoğlan et al., 2016; Rızaoğlu et al., 2006, 2009; Topuz et al., 2017). Based on the available geochronological data, Schleiffarth et al. (2018) inferred that there is a magmatic quiescence between 72 and 58 Ma. In addition to this continental arc magmatism, several igneous complexes located near the Bitlis Suture, such as Yüksekova and Helete complexes, have been interpreted as remnants of an accreted intraoceanic arc and its backarc basin, mainly based on the tholeiitic affinity of the igneous rocks (Beyarslan & Bingöl, 2018; Ertürk, 2025; Nurlu et al., 2015; Sar et al., 2019; Ural et al., 2015, 2021). The Helete Complex, exposed ∼10–15 km north of the Kastel Formation, is intruded by a suite of tholeiitic tonalite–trondhjemite–granodiorite bodies dated to 93–84 Ma (2σ; Nurlu et al., 2015; Robertson & Parlak, 2025). Associated radiolarian cherts yield late Cenomanian–Campanian ages, while planktonic foraminifera in micritic limestones indicate deposition from the late Campanian to late Maastrichtian (Ural et al., 2015, 2022; Ural & Sari, 2019). The age range of these "intraoceanic arc" assemblages partially overlaps with that of the continental arc. However, the spatial extent of this proposed "intraoceanic arc" (including its width and lateral continuity) and the timing of its accretion remain uncertain, underscoring the need for additional field constraints. Another complication in the geology of SE Anatolia is the presence of tholeiitic gabbroic rocks (87–83 Ma) in the Ispendere, Kömürhan, and Göksun areas, commonly interpreted as components of a supra-subduction zone ophiolite (e.g., Bingöl et al., 2018; Karaoğlan et al., 2012; Parlak, 2016; Rızaoğlu et al., 2006). However, their close association with coeval high-K calc-alkaline granitoids suggests an arc-related igneous origin rather than obducted fragments of oceanic lithosphere (Dicheng Zhu, pers. comm., 2018).

The Late Cretaceous H*T*-L*P* metamorphic rocks and intrusions were exhumed to the Earth's surface by Maastrichtian, as they were unconformably overlain by Maastrichtian reefal limestones (Figure 5; e.g., Topuz et al., 2017; Yılmaz et al., 2023). This rapid exhumation is attributed to extensional processes driven by slab pull of the subducting northern Neo-Tethys oceanic lithosphere (e.g., Gün et al., 2021). The Maastrichtian reefal limestones were locally overlain by lower Paleocene distal alluvial fan deposits (Türkmen, 2004). After the deposition of the Maastrichtian reefal limestones, the Eastern Anatolia was uplifted above sea level. A major marine transgression during the middle Eocene led to deposition of a thick siliciclastic–carbonate succession consisting of sandstone, marl, and limestone. Renewed uplift during the late Eocene again exposed the region subaerially. Sparse apatite fission-track ages from Eastern Anatolia range between 53 and 36 Ma, consistent with Eocene cooling and exhumation (Albino et al., 2014; Cavazza et al., 2018; Karaoğlan et al., 2016). Contemporaneous Eocene volcanism was localized along the Bitlis Suture (Ertürk et al., 2018; Karaoğlan et al., 2013) and within ∼30 km south of the İzmir–Ankara–Erzincan Suture (Okay et al., 2022; Topuz et al., 2011). Toward the late Rupelian, another large-scale marine transgression deposited a thick turbiditic succession that grades upward into shallow-marine sandstone, shale, and limestone of Early Miocene age (Okay et al., 2010, 2020b; Yılmaz et al., 2023; Özcan et al., 2010). During the Middle Miocene, Eastern Anatolia was uplifted once more above sea level, after which no further marine transgressions occurred, while the Bitlis Suture Zone experienced rapid cooling and exhumation interpreted as the result of the Arabia–Eurasia hard collision (Cavazza et al., 2018; Okay et al., 2010; Robertson & Parlak, 2025). From the Early Miocene to the Quaternary, magmatism was widespread across the region (Açlan & Altun, 2018; Keskin, 2003; Keskin et al., 1998; Pearce et al., 1990; Schleiffarth et al., 2018; Topuz et al., 2019; Çubukçu et al., 2012; Özdemir & Güleç, 2014).

2.3. Bitlis Suture Zone

The Bitlis–Pütürge Massif is a Late Cretaceous metamorphic belt composed primarily of amphibolite-facies micaschist, ortho- and paragneiss, and marble, with locally preserved eclogite lenses and blueschist-facies slivers (Oberhänsli et al., 2010, 2013; Okay et al., 1985). The orthogneisses were derived from granitic intrusions with igneous crystallisation ages of 572–531 Ma (Beyarslan et al., 2016; Ustaömer et al., 2009, 2012). The metamorphism is dated to the Late Cretaceous, with U–Pb metamorphic zircon ages ranging from 84 to 82 Ma and $^{40}Ar/^{39}Ar$ muscovite ages between 79 and 74 Ma (Oberhänsli et al., 2010, 2013). The Bitlis-Pütürge Massif contains a similar suite of continental rocks, with U–Pb rutile ages of ca. 80 Ma (Şimşek et al., 2024, 2025). The Bitlis-Pütürge Massif can be regarded as a product of continental subduction, as it contains continental rock assemblages. In contrast to the East Anatolian Plateau, where apatite fission-track ages are predominantly Eocene (e.g., Albino et al., 2014; Cavazza et al., 2018; Karaoğlan et al., 2016), the Bitlis-Pütürge Massif shows apatite fission-track ages between 13 and 18 Ma (Cavazza et al., 2018; Karaoğlan et al., 2016; Okay et al., 2010). These data indicate that the Bitlis-Pütürge Massif experienced significant uplift during the Mid-Miocene. This Mid-Miocene uplift broadly coincides with the deepening of the Arabian Foreland Basin during the Early

Table 2
UTM Coordinates of the Samples Used for U–Pb and Hf Isotopic Analyses, Along With the Corresponding Number of Analyses for Each Sample

			Coordinates UTM (37S)		Zircon			
Sample	Formation	Stratigraphic age	Easting	Northing	Total analyses	Concordant analyses	Hf isotope analyses	REE analyses
518	Kastel	late Campanian	0404861	4174881	135	108	106	–
519	Kastel	late Campanian	0403315	4174100	57	35	31	–
1017	Kastel	late Campanian	0403650	4175432	120	108	–	120
1028	Kastel	late Campanian	0403361	4175655	42	30	–	42
1057	Germav	early Paleocene	0404462	4177563	120	104	–	120
1112	Germav	early Paleocene	0453729	4201513	120	62	–	120
				Total	594	447	137	402

Miocene (see above). The Bitlis-Pütürge Massif was already at the Earth's surface by the Eocene, as deduced from the local presence of Eocene volcanic rocks on metamorphic rocks, and was subsequently reburied during the Eocene. There are two main intact ophiolite slices, such as Kızıldağ and Guleman, and a Late Cretaceous ophiolithic mélange (Koçali Complex) obducted on the leading edge of the Arabian Platform. These ophiolites and plagiogranite in the Koçali Complex were dated as 96–92 Ma by U–Pb zircon (e.g., Bingöl et al., 2018; Dilek & Thy, 2009; Karaoğlan et al., 2013). The ages of deep-marine sedimentary blocks within the ophiolitic mélanges range from the Late Triassic to early Late Cretaceous (e.g., Tekin et al., 2011; Uzunçimen et al., 2011; Varol et al., 2011), indicating that the oceanic domain existed at least since the Late Triassic. As noted above, the timing of the obduction is constrained to be mid-to late Campanian, as the ophiolites are unconformably overlain by upper Campanian-lower Maastrichtian non-marine to shallow-marine sedimentary rocks (Figure 3; e.g., Terbüzek and Besni formations; Steuber & Schlüter, 2012; Robertson et al., 2016, and references therein; Özer, 2025).

3. Analytical Techniques

In this study, we conducted modal analysis of sandstone samples, micropaleontological identification of planktonic foraminifera and calcareous nannoplankton in mudstones, and U–Pb dating of detrital zircons from sandstones, combined with trace element analyses and in-situ Hf isotopic measurements. The analytical procedures are described in detail in Supporting Information S1. The stratigraphic ages of the investigated clastic rocks range from Campanian to Paleocene, as shown in Figure 3. Table 2 lists UTM coordinates of the samples used for U–Pb and Hf isotopic analyses, along with the corresponding number of analyses for each sample.

Modal analyses were performed on 10 samples of upper Campanian to early Maastrichtian sandstones from the Kastel Formation. For each sample, at least 500 points were counted following the Gazzi–Dickinson method (Dickinson, 1970; Zuffa, 1985; Table S1). In addition, two sandstone samples from upper Maastrichtian to lower Paleocene calciturbidites of the Germav Formation, which were used for U–Pb geochronology, were also examined petrographically. Planktonic foraminifera were identified either in thin sections or from washed residues of a total of 22 samples from the Kastel and Germav formations. To obtain free planktonic foraminifera, the samples were disaggregated by treatment with dilute hydrogen peroxide (30%) and acetic acid (80%). The abundance of planktonic foraminiferal assemblages varies widely from very low to moderate; preservation is moderate to good in some samples, but poor in most. The distribution of planktonic foraminiferal species and scanning electron microscope (SEM) images of selected planktonic foraminifera species are provided in Table S2; Figures S1a–S1c in Supporting Information S1. For the study of calcareous nannofossil assemblages, 20 samples were prepared as simple smear slides following standard techniques and analyzed under light microscopy at 1,250 magnification. Data were collected using the semiquantitative counting method described by Backman and Shackleton (1983). The abundance of calcareous nannofossils was determined by counting the number of specimens in a prefixed area corresponding to 2 mm^2. The taxonomic list of taxa considered in the present study can be found in Table S3; Figure S4 in Supporting Information S1.

10.1029/2025TC009243

Zircons were extracted from the sandstone samples using standard mineral separation techniques, including crushing, milling, sieving, and rinsing. Nonmagnetic mineral fractions were then isolated using a magnetic separator. Subsequently, heavy mineral fractions were separated from the nonmagnetic concentrates using heavy liquid separation with sodium polytungstate. Special care was taken in order to achieve unbiased handpicking of zircon grains (e.g., independent of size, shape, color, degree of rounding, and transparency). The randomly selected grains were mounted on adhesive tape, embedded in a 25 mm diameter epoxy mount, and subsequently lapped using 2,500-mesh SiC paper. Final polishing was performed using 9, 3, and 1 μm diamond suspensions. Internal structures of the mounted zircons of two samples (518 and 519) were imaged using cathodoluminescence (CL) with a Carl Zeiss Supra 55 field-emission scanning electron microscope (FE-SEM) coupled to a GATAN MonoCL4 detector at the State Key Laboratory for Mineral Deposits Research in Nanjing University, China. The analysis conditions were an accelerating voltage of 7 kV, a working distance of 11.8 mm, and an aperture size of 30 μm. CL images of the other four samples (1017, 1028, 1057, and 1112) were produced using a Tescan GAIA 3 field-emission scanning electron microscope (FE-SEM) at Hacettepe University in Türkiye. The analysis conditions were an accelerating voltage of 20 kV and a working distance of 10 mm. The CL images of the analyzed zircons are given in Figures S3a–S3c of Supporting Information S1. U-Pb dating of detrital zircons from samples 518 and 519 was performed using a ThermoFisher Scientific iCAP RQ ICP-MS coupled to a Geolas 193 nm laser ablation system at the State Key Laboratory for Mineral Deposits Research of Nanjing University (MiDeR-NJU). On the other hand, U–Pb dating of detrital zircons from samples 1017, 1028, 1057 and 1112 was conducted using LA-ICPMS in Nanjing Hongchuang Exploration Technology Service Co., Ltd. Zircon Hf isotopic analyses were performed at the State Key Laboratory for Mineral Deposits Research, Nanjing University, using a Neptune Plus MC-ICP-MS coupled to an ESI NWR193HE laser ablation system.

4. Results

4.1. Petrography

Samples 518, 519, 1017, and 1028 from lower horizons of upper Campanian–lower Maastrichtian strata of the Kastel Formation (Figure 3) are fine- to medium-grained, poorly sorted lithic arenites composed predominantly of rock fragments and calcite, with minor amounts of plagioclase (locally entirely replaced by calcite), quartz, Cr-spinel, and muscovite (Figures 6a–6d). Lithic fragments are the dominant component, comprising ca. 60%–80% of the total volume, and are represented by serpentinite, limestone, microdiorite, and acidic volcanic rocks. Notably, serpentinite grains are significantly coarser than felsic volcanic rock fragments as well as quartz and feldspar grains (Figures 6a–6c). The grains are angular to subangular in shape, with sizes ranging from 50 to 400 μm, reflecting the poorly sorted character of the sandstone. These features collectively indicate a low degree of both textural and mineralogical maturity.

Sample 1058, a silty packstone from the basal levels of the late Maastrichtian–Paleocene Germav Formation (Figures 3 and 6e), is dominated by planktonic foraminifera with 10–20 vol.% rock fragments, largely derived from acidic volcanic sources with minor limestone contributions. In contrast, sample 1112, collected from the upper Germav Formation, is a poorly sorted lithic sandstone composed of ~70 vol.% rock fragments, ~5 vol.% quartz, ~3 vol.% feldspar, and ~2 vol.% glauconite, set in a fine-grained carbonate matrix (~20 vol.%; Figure 6f). The grains are angular to subangular, with sizes ranging from 70 to 300 μm. Comparable to sandstones of the Kastel Formation, the textural and mineralogical features of sample 1112 indicate low compositional and textural maturity, consistent with deposition in a high-energy, proximal sedimentary setting.

4.2. Biostratigraphy and Maximum Depositional Ages

The biostratigraphy of the Kastel and Germav formations was investigated based on planktonic foraminiferal and calcareous nannoplankton assemblages identified in mudstone and sandstone samples. The stratigraphic positions of the studied samples are shown in Figure 3. Tables S2 and S3 summarize the identified planktonic foraminiferal taxa and calcareous nannofossils from the Kastel and Germav formations, respectively. Scanning electron microscope (SEM) images of the identified planktonic foraminifera are presented in Figures S1a–S1c of Supporting Information S1, while photomicrographs of the nannoplankton are shown in Figure S2 of Supporting Information S1.

The Kastel Formation conformably overlies pelagic limestones (Figure 3), and its lower horizons are dominated by mudstone. Up-section, the succession grades into alternating mudstone and sandstone layers, with a

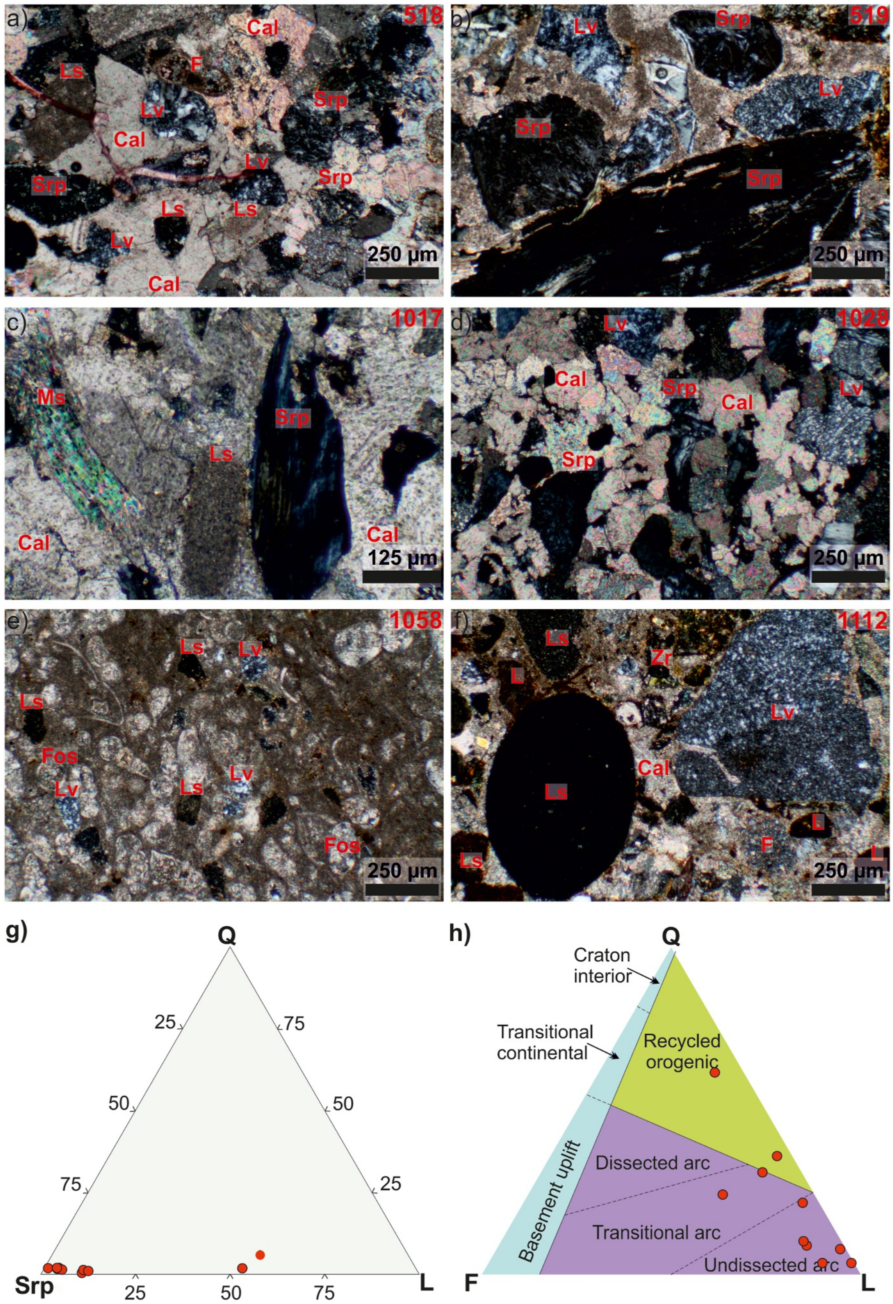

Figure 6. Representative micrographs illustrating the textural and mineralogical features of the studied rock samples under crossed polars. Samples 518 (a), 519 (b), 1017 (c), and 1028 (d) are lithic sandstones from the Kastel Formation. Sample 1058 (e) is a silty packstone, and sample 1,112 (f) is lithic sandstone from the Germav Formation. (g–h) Point-counting results of sandstone samples from the Kastel Formation plotted on triangular diagrams: (g) Quartz–Serpentinite–Lithic fragments (excluding serpentinite); and (h) Quartz–Feldspar–Lithic fragments (after Dickinson et al., 1983). Q Quartz, F Feldspar, L Lithic fragment, Ls Sedimentary rock fragment, Lv Volcanic rock fragment, Cal Calcite, Fos Fossil fragment, Ms Muscovite, Zr Zircon, Srp Serpentine.

progressive increase in sandstone thickness and a decrease in mudstone content. This vertical change suggests an upward-shallowing depositional environment. Additionally, the formation is capped by continental deposits overlying an erosional surface. In contrast, the Germav Formation was deposited in a deeper marine environment above rudist-bearing limestones, with a sharp boundary separating the two units.

Planktonic foraminifera assemblages from the basal mudstone layers of the Kastel Formation suggest a latest Campanian–early Maastrichtian depositional age (73–71 Ma; Gradstein et al., 2012), based on the identification of the *Gansserina gansseri* Zone (Premoli Silva & Verga, 2004). Consistently, calcareous nannofossils from the same samples correspond to Zone CC23a (Perch-Nielsen, 1985), which is correlated with an age interval of ca. 74–71 Ma (Gardin et al., 2012). The lowermost calciturbidite layers of the Germav Formation, deposited on a hardground surface above the neritic carbonates of the Besni Formation, contain late Maastrichtian planktonic assemblages. A few centimeters higher in the section, starting from sample 1059, planktonic foraminifera assemblages correspond to the P1b Subzone (Wade et al., 2011), indicating Danian depositional ages (∼64.3–62.9 Ma). In parallel, calcareous nannofossils from these same samples indicate Zone CNP4 of the early Paleocene (ca. 62.6 Ma; Agnini et al., 2014).

In summary, the biostratigraphic age determinations indicate that the Kastel Formation was deposited during the late Campanian to early Maastrichtian, while the Germav Formation spans the late Maastrichtian to early Paleocene. These age constraints are roughly consistent with those previously reported by Robertson et al. (2016). The dated samples from the Kastel Formation indicate depositional ages of 74–71 Ma, whereas the samples from the Germav Formation were deposited around 64–63 Ma.

4.3. Zircon Morphology and Internal Structure

The zircon grains in the studied samples range from 50 to 250 μm in length. Their colors vary from clear and transparent to yellowish. Grain morphologies range from nearly euhedral to fully rounded. The majority of the grains (ca. 80%) exhibit euhedral to subhedral forms, while rounded zircons are relatively rare. Notably, sample 1057 from the Germav Formation contains a higher proportion of rounded grains (∼35% of the population). Cathodoluminescence (CL) images of the zircon grains predominantly exhibit well-defined oscillatory and sector zoning in ca. 80% of the grains (Figures S3a–S3c in Supporting Information S1). In some instances, the pale CL intensity locally masks the oscillatory zoning. Unzoned interiors and metamict domains are more commonly observed in zircon grains from the Germav Formation. Inclusions of apatite, feldspar, and plagioclase are common. For the measurement, we mostly preferred marginal domains of the zircon grains.

4.4. Trace Element Compositions

Trace element compositions of detrital zircon grains were obtained from 402 spot analyses conducted concurrently with U–Pb dating on four samples (Table 2). Of these, only the 294 analyses with concordant U–Pb ages—defined by a (^{207}Pb/^{235}U age)/(^{206}Pb/^{238}U age) × 100 ratio between 90% and 110%—are considered for further interpretation (Table S5).

The zircon grains are predominantly characterized by steep, heavy rare earth element (REE)-enriched patterns, a pronounced positive Ce anomaly, and a distinct negative Eu anomaly (Table S5; Figure S4 in Supporting Information S1). Chondrite-normalized Yb/Gd values range from 7 to 40, and Eu/Eu* values vary between 0.01 and 0.80. Only four grains have Eu/Eu* values ranging from 0.84 to 1.01, suggesting that most dated zircon grains crystallized in the presence of plagioclase and in the absence of garnet. Some analyses on zircon grains with concordant ages show elevated concentrations of P, Fe, and La, accompanied by a reduced Ce/Ce* anomaly. This feature likely results from the presence of mineral inclusions within the zircon grains.

Th/U ratios of zircon grains with concordant ages range from 0.10 to 3.47. Only two grains exhibit exceptionally high Th/U ratios (285 and 313), while four grains have ratios between 0.10 and 0.15. The majority of zircon grains (∼96%) display Th/U ratios between 0.15 and 1.0 (Figure S5 in Supporting Information S1). Generally, zircon grains with Th/U values below 0.10 are interpreted to be of metamorphic origin, and those with values above 0.10 are of igneous origin (e.g., Belousova et al., 2002; Hoskin & Ireland, 2000; Hoskin & Schaltegger, 2003; Rubatto, 2002). However, Yakymchuk et al. (2018) emphasized that Th/U ratios in zircon are influenced by multiple factors, including (a) the absolute concentrations of Th and U, (b) the abundance of monazite in the system, and (c) the timing of zircon crystallization. Not all metamorphic zircon grains necessarily exhibit Th/U < 0.10. Considering the internal zoning patterns and the specific conditions required for metamorphic zircon growth, we infer that the vast majority of the zircon grains analyzed in this study are from felsic igneous rocks, and those of metamorphic origin are minimal.

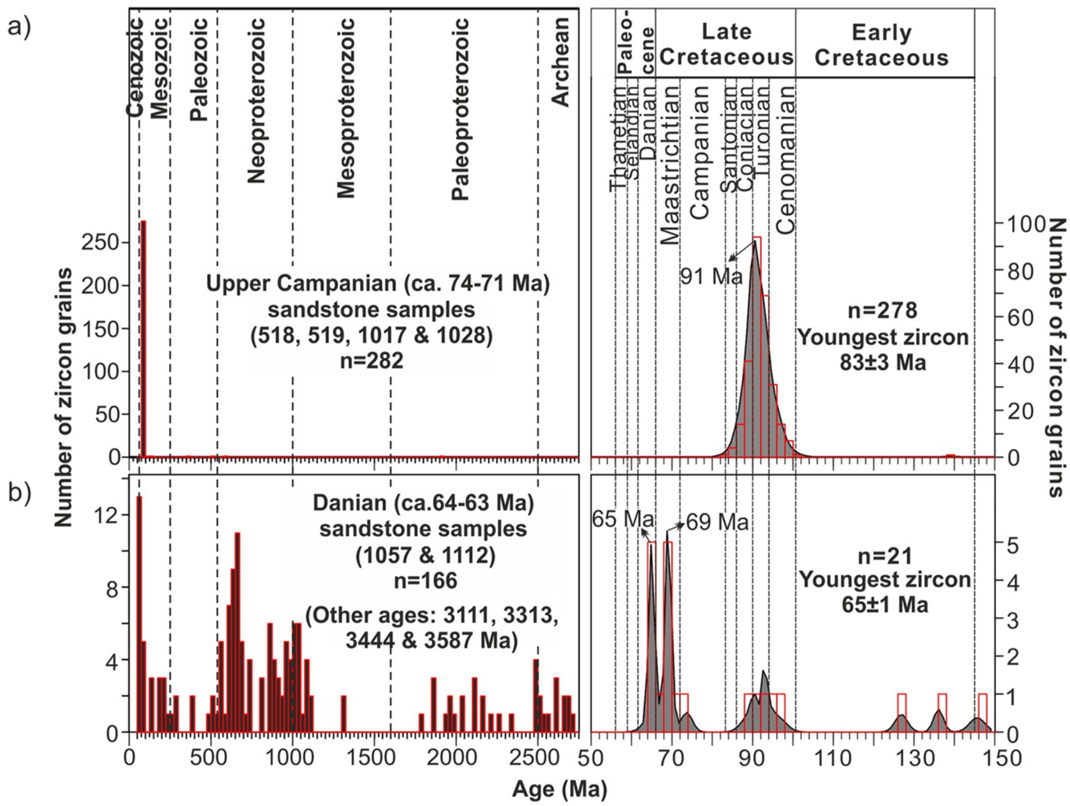

Figure 7. Detrital zircon age histograms of the sandstone samples from the (a) Kastel and (b) Germav formations. Cretaceous-Paleocene zircons are shown on the right-hand panels.

4.5. U–Pb Detrital Zircon Chronology

A total of 594 U–Pb LA-ICP-MS spot analyses were conducted on six samples (Table 2). Of these, 447 zircon grains yielded concordant U–Pb ages within the 90%–110% concordance range. This corresponds to ca. 75% of the total analyses (Table S4). Detrital zircon age histograms for each sample are presented in Figure S6 of Supporting Information S1.

All four samples of upper Campanian–lower Maastrichtian sandstone (samples 518, 519, 1017, and 1028; Kastel Formation) yielded comparable detrital zircon age spectra. The obtained ages range from 83 to 1,909 Ma, with approximately 98% of all the concordant ages falling between 83 and 103 Ma, and a prominent age peak at 94–90 Ma (Figure 7a; Table S4). Only five zircon grains yielded older ages, which are scattered and do not exhibit significant clustering. The youngest detrital zircon ages from these samples range from 83 ± 3 Ma to 88 ± 2 Ma (2σ). Maximum depositional ages, calculated using the AgePick software (Dickinson & Gehrels, 2009; Gehrels, 2014) based on the weighted mean of the youngest age cluster, range from 83 to 86 Ma (Table S6). These values are notably older than the biostratigraphic age of the formation (ca. 74–71 Ma).

Two samples of lower Paleocene sandstone (samples 1057 and 1112; Germav Formation) yielded 166 concordant zircon ages. The $^{206}Pb/^{238}U$ ages range from 65 ± 1 Ma to 3,587 ± 13 Ma (2σ). In contrast to the detrital zircon age spectra from the upper Campanian–lower Maastrichtian sandstone samples, these spectra display prominent age clusters at: Late Cretaceous–early Paleocene (100–65 Ma, 11% of total concordant grains), late Neoproterozoic–Cambrian (750–500 Ma, 28%), late Mesoproterozoic–early Neoproterozoic (1,100–800 Ma, 28%), Paleoproterozoic (2,340–1,790 Ma, 11%), and late Paleoproterozoic–early Archean (2,710–2,490 Ma, 10%; Figure 7b; Table S4). Additionally, a minor component of scattered Paleozoic–Mesozoic zircon grains (11%) is present. The youngest detrital zircon ages are 65 ± 1 Ma and 65 ± 4 Ma (2σ), consistent with the Danian age inferred from biostratigraphic data (64–63 Ma).

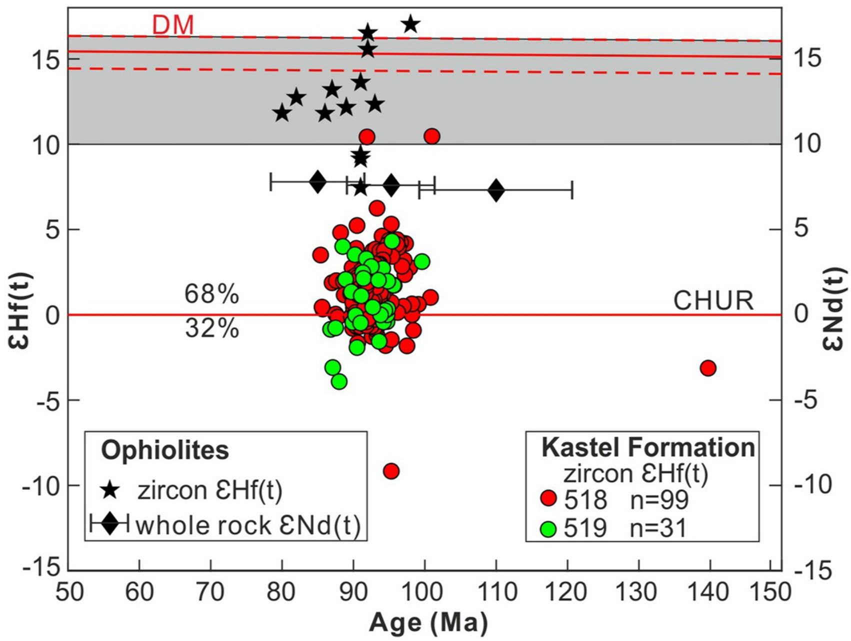

Figure 8. U-Pb zircon ages plotted against εHf(t) values for detrital zircon grains from upper Campanian–lower Maastrichtian sandstones of the Kastel Formation. Only grains with ages between 85 and 140 Ma are shown. Three older zircons (1909, 575, and 366 Ma) yield εHf(t) values of −7, −1, and 0, respectively. For comparison, εHf(t) values of zircons (Bingöl et al., 2018) and εNd(t) whole-rock values (Karaoğlan et al., 2012, 2013) from plagiogranite and gabbro samples of ophiolitic rocks in southeastern Türkiye are also included. In addition, the field of the initial εHf values of zircons from well-documented intraoceanic arcs such as Izu-Bonin (Schmitt et al., 2018) and Kohistan (Ewing & Müntener, 2018; Schaltegger et al., 2002) is shown in gray. DM, Depleted Mantle; CHUR, Chondritic Uniform Reservoir.

To summarize, the detrital zircon populations from the upper Campanian (ca. 74-71 Ma) and lower Paleocene (ca. 64-63 Ma) sandstones exhibit markedly different age spectra. The zircon grains from the upper Campanian sandstones define a single prominent Late Cretaceous age cluster, peaking between 94 and 90 Ma. In contrast, the zircon grains from the lower Paleocene sandstone display a more diverse age distribution, including a substantial proportion of Neoproterozoic grains, together with Late Cretaceous and Paleocene zircons.

4.6. Lu-Hf Isotope Compositions

A total of 133 concordant zircon grains from two upper Campanian sandstone samples (518 and 519) were analyzed for their Lu-Hf isotopic compositions (Table 2). The results are presented in Table S7.

The εHf(t) values of the zircon grains range from −9.2 to +10.5, with ca. 95% of the grains falling between −3.9 and + 5.3 (Figure 8; Table S7). Only three grains yielded εHf(t) values greater than +5.5 (6.2, 10.4, and 10.5). Zircons from sample 519 exhibit a higher proportion of negative εHf(t) values (35% of analyzed grains) compared to the stratigraphically older sample 518 (25%). Overall, ca. 32% of the Late Cretaceous zircon grains are characterized by negative εHf(t) values.

A comparison with the εHf(t) values of igneous zircon grains from plagiogranite and diabase units of the Kızıldağ ophiolite reveals that zircons from the 96–92 Ma suprasubduction-zone ophiolite exhibit distinctly positive εHf(t) values, ranging between +10 and + 15 (Figure 8; e.g., Bingöl et al., 2018; only εHf(t) values of concordant zircon grains were considered from the reference data set). Similarly, εNd(t) values of gabbroic rocks from the Kızıldağ ophiolite range from +6 to +8 (Karaoğlan et al., 2012, 2013). Within our data set, only two zircon grains yield εHf (t) values that overlap with those of the 96–92 Ma ophiolitic rocks. In contrast, a substantial proportion of the Late Cretaceous zircon grains in our samples (ca. 32%) exhibit negative εHf(t) values, suggesting derivation from magmas that incorporated significant amounts of older continental crustal material during their genesis.

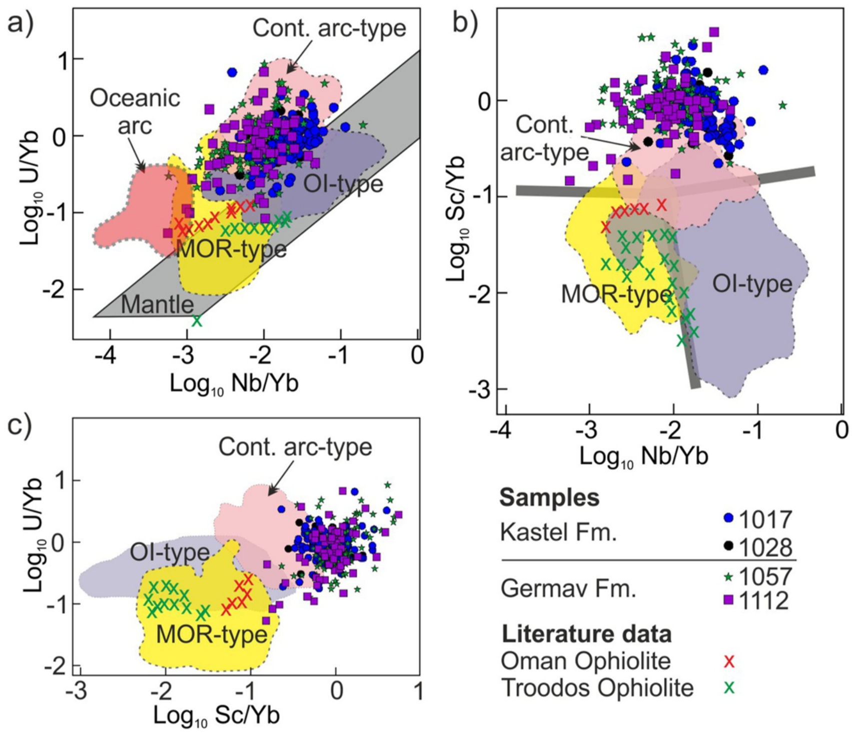

Figure 9. Tectonic discrimination diagrams after Grimes et al. (2015), based on U/Yb, Sc/Yb, and Nb/Yb ratios of detrital zircons (a–c). Zircons from the Kastel Formation plot distinctly from those of the Troodos and Oman ophiolites (shown as green and red crosses, respectively; Grimes et al., 2015), supporting a continental arc origin for the Kastel zircons. The compositional field for zircons from the oceanic arc (Izu-Bonin) in Log_{10}Nb/Yb versus Log_{10}U/Yb (a) is taken from Schmitt et al. (2018). Because Sc data are not available, the compositional fields for oceanic-arc zircons are unconstrained in diagrams (b, c). Ol-type: Oceanic island type; MOR-type, Mid-ocean ridge type; Cont. arc-type, Continental arc type.

5. Discussion

5.1. Sandstone Provenance Interpretation and Timing of the Continental Collision

As pointed out above, both the internal structure and geochemical features of the detrital zircons from the sandstones of the Kastel and Germav formations suggest an origin from igneous sources, with minimal metamorphic input. Grimes et al. (2015) demonstrated that zircons crystallized in orogenic igneous settings can be distinguished from those formed in oceanic island and mid-ocean ridge environments based on Nb/Yb versus U/Yb, Nb/Yb versus Sc/Yb, and Sc/Yb versus U/Yb plots (Figure 9). The zircon grains from the upper Campanian sandstones (the Kastel Formation) plot within the compositional field typical of continental arc settings. However, the sandstones of the Kastel Formation also contain abundant serpentinite clasts and Cr-spinel grains, indicating a significant contribution from ophiolitic sources. The abundance of ophiolitic detritus in these sandstones led Robertson et al. (2016) and Robertson and Parlak (2025) to propose that the Kastel sandstones were predominantly sourced from the obducted ophiolitic complexes and accreted intraoceanic arc. However, this interpretation is at odds with the εHf(t) values of the detrital zircons with ages of 100–85 Ma, which range from −3.9 to +5.3, with a significant proportion (~32%) displaying negative values. These values contrast markedly with the highly positive εHf(t) values (+7 to +16) of zircons from the 92–96 Ma ophiolite (Figure 8; Bingöl et al., 2018), and juvenile intraoceanic arcs such as Izu-Bonin and Kohistan (Figure 8; Ewing & Müntener, 2018; Schaltegger et al., 2002; Schmitt et al., 2018). Furthermore, zircons from the juvenile oceanic arcs are characterized by low U/Yb and Nb/Yb ratios compared to those from the continental arcs (Figure 9a). Thus, we consider it unlikely that the detrital zircons were derived predominantly from ophiolitic sources or an intra-oceanic arc, based on their age range, compositional characteristics, and initial isotopic compositions. The apparent dominance of ophiolitic detritus in the Kastel Formation is more plausibly explained by the close proximity of obducted ophiolitic rocks to the depositional site. This interpretation is supported by the relatively coarse grain size of serpentinite clasts (Figures 6a–6c), despite their limited durability during prolonged transport. We posit that the low proportion of felsic volcanic rocks, quartzo-feldspathic and muscovite grains, clearly derived from continental crust, likely reflects dilution by abundant ophiolitic lithic fragments, whereas zircon grains were probably preserved and transported owing to high durability.

The Arabian Platform was a passive continental margin and lacks any record of Paleozoic and Mesozoic magmatism, as noted above. Therefore, the Arabian Platform can be excluded as a potential source for the Late Cretaceous detrital zircons. Eastern Anatolia, to the north of the Bitlis Suture, hosts a Late Cretaceous magmatic arc developed atop a continental basement, the Baskil magmatic arc (Figures 1 and 2; Ertürk et al., 2022; Liu et al., 2022; Kuşcu et al., 2013; Rızaoğlu et al., 2009; Topuz et al., 2017; Yazgan, 1984; Yazgan & Chessex, 1991). However, the age of the arc-related igneous rocks dated so far in this continental domain are slightly younger, ranging from 87 to 69 Ma, different from the primary age population of detrital zircon grains from the Kastel Formation, which peaks at approximately 91 Ma. Only the Helete Complex, interpreted as an oceanic arc located ∼10–15 km north of the Kastel Formation, contains intrusive rocks ranging from gabbro to granite dated at 93–84 Ma (Nurlu et al., 2015; Robertson & Parlak, 2025). These rocks show predominantly positive initial whole-rock εNd(t) values (+6 to +8), which correspond to εHf(t) values of +10 to +14 based on the terrestrial array of Vervoort et al. (2011). Such values are systematically higher than most εHf(t) values measured in detrital zircons from the Kastel Formation, arguing against a dominant contribution from the Helete Complex.

In marked contrast to the detrital zircon age spectra of the sandstones from the Kastel Formation, those from the Danian Germav Formation are dominated by Cambrian and Precambrian zircon grains (ca. 87% of the concordant zircons), while Late Cretaceous–early Paleocene zircon grains (100–65 Ma) are subordinate (ca. 11%; Figure 7; Figure S6 in Supporting Information S1). The Cambrian and Precambrian zircon grains in the Germav Formation sandstones may have been sourced from the basement rocks of the Arabian Platform, the Anatolide–Tauride Block, and the Bitlis–Pütürge Massif (Beyarslan et al., 2016; Gürsu et al., 2015; Topuz et al., 2017; Ustaömer et al., 2009, 2012). However, the Arabian Platform is considered a less probable source, as paleocurrent data from both the Kastel and Germav formations consistently indicate sediment transport from the north (Robertson et al., 2016). The age spectra of the Danian samples can be explained by feeding primarily from an older continental basement rocks rather than from a contemporaneous magmatic arc. Cawood et al. (2012) demonstrated that detrital zircon age spectra in sandstones are indicative of their tectonic setting. Sandstones from foreland basins, trenches, and forearc settings typically contain high proportions of zircons close to the depositional age. In contrast, sandstones from collisional, extensional, and intracratonic settings tend to have larger proportions of older zircons derived from basement rocks (see also Yılmazer et al., 2025). Accordingly, the detrital zircon age spectra of the upper Campanian Kastel Formation resemble those characteristic of active arc settings. The temporal discrepancy between the depositional age of the Kastel Formation (74–71 Ma) and the youngest detrital zircon grains it contains (83 ± 3 Ma) is noteworthy. A detailed examination of the age distribution of igneous rocks north of the suture indicates that magmatism dated at 77–69 Ma is restricted to a relatively limited area north of the Anatolide–Tauride Block (Figure 2), whereas regions closer to the suture, are dominated by igneous rocks with ages of 93–81 Ma (Figure 2). We therefore infer that the absence of zircon grains younger than 83 ± 3 Ma reflects the lack of younger igneous sources within the sediment catchment area. In contrast, the age spectra from the Danian Germav Formation resemble those typical of collisional settings (see Figures 7a and 7b), characterized by a high proportion of Cambrian and Precambrian zircon grains in addition to Late Cretaceous–early Paleocene populations. By Danian time, the Bitlis-Pütürge Massif had been exhumed to the Earth's surface, and the upper crustal sections of the Late Cretaceous magmatic arc had been largely removed by erosion. This tectonic configuration would have supplied substantial quantities of Precambrian zircons from the Bitlis-Pütürge Massif and the Malatya-Keban metamorphic rocks.

In summary, the detrital zircons in the upper Campanian sandstones of the Arabian Platform (Kastel Formation) were primarily sourced from a Late Cretaceous Baskil magmatic arc. The notable presence of basement-derived zircons in the Danian sandstones (Germav Formation) indicates exhumation of the Bitlis-Pütürge Massif and the Malatya and Keban metamorphic rocks at the Earth's surface by the Danian. Consequently, the continental collision between the Arabian Platform and the Anatolide–Tauride Block must have taken place definitively before the Danian, probably during the late Campanian. This estimate is comparable to that proposed by Berberian and King (1981), Yazgan (1984) and Yazgan and Chessex (1991) (Table 1). However, further provenance studies along the Bitlis Suture may help to better constrain the timing, given the limited geographic extent of the study area. The ophiolite obduction onto the Arabian Platform occurred approximately synchronously with continental collision, a temporal relationship that is not universal elsewhere.

5.2. Geodynamic Models and Further Evidence for Late Cretaceous Collision

The main challenge lies in the wide range of proposed ages for the collision, spanning from the Late Cretaceous to the Miocene. A key issue underlying this discrepancy is the debated position and tectonic role of the Bitlis-Pütürge Massif. Consequently, there are numerous contrasting interpretations in the literature regarding the timing of collision and/or closure of the southern branch of the Neo-Tethys. These differing interpretations reflect fundamentally distinct geodynamic models, which can be broadly grouped into three end-member scenarios.

In the most widely accepted scenario, the Bitlis-Pütürge Massif is regarded as an independent continental microplate located between the Arabian Platform and the Anatolide–Tauride Block, bounded by suture zones to both the north and south (e.g., Oberhänsli et al., 2010, 2013; Robertson et al., 2006, 2012; Şengör et al., 2008; Figure 2). In this framework, accretion of the Bitlis–Pütürge Massif to the Anatolide–Tauride Block is considered to have occurred during the Late Cretaceous, whereas closure of the oceanic domain south of the massif, represented by the Bitlis Thrust, is attributed to the Miocene time. The main argument put forward by studies suggesting a Miocene continental collision is based on enhanced subsidence of the Arabian Platform during the Early Miocene, recorded by the Lice Formation, together with apatite fission-track ages of 18–13 Ma from the Bitlis-Pütürge Massif (e.g., Cavazza et al., 2018; Okay et al., 2010). However, this tectonic scenario fails to explain the presence of Late Cretaceous detrital zircons in Upper Campanian to Lower Paleocene clastic deposits of the Arabian Foreland Basin. The enhanced Early Miocene subsidence of the Arabian Foreland Basin, inferred from reefal carbonates grading upward into siliciclastic marine turbidites, may instead reflect coeval uplift and thrusting of the Bitlis–Pütürge Massif along the Bitlis Thrust onto the Arabian Platform (Figure 2). We interpret this thrusting and associated deepening of the Arabian Platform in front of the Bitlis Thrust as a consequence of continued convergence following continental collision. Further evidence arguing against a Miocene collision includes the absence of mélange complexes and high-pressure metamorphic rocks younger than Late Cretaceous. Moreover, the region lacks Paleocene, Eocene, or Oligocene arc magmatism, which would be expected if subduction and continental collision had persisted into the Miocene.

The second end-member scenario interprets the Bitlis–Pütürge Massif as part of the southern margin of the Anatolide-Tauride Block (van Hinsbergen et al., 2020). In this model, the Bitlis–Pütürge Massif occupied a more distal position along the margin than the Keban Metamorphics and was subsequently underthrust to greater depths during convergence. Within this framework, the massif is considered to have been overthrust by Cretaceous ophiolites and to have experienced Late Cretaceous metamorphism following ophiolite emplacement. Northward obduction of the Cretaceous ophiolites onto the southern Bitlis–Pütürge and Keban blocks is further invoked to explain a northward decrease in metamorphic grade. However, this model is difficult to reconcile with key observations. Peak metamorphism in the Bitlis-Pütürge Massif (84–82 Ma) predates the inferred timing of ophiolite emplacement (middle to late Campanian, 80–72 Ma). Moreover, the occurrence of retrogressed eclogites and blueschists within the Bitlis–Pütürge Massif indicates involvement in subduction processes, which is not adequately explained by this model.

In the third end-member scenario, which we adopt here (Figure 10), the Bitlis–Pütürge Massif is interpreted as the subducted northern margin of the Arabian Plate, with the main suture zone located to the north of the massif (e.g., Yazgan, 1984; Yazgan & Chessex, 1991). In this scenario, the massif does not represent an independent block but rather a structurally reworked segment of the Arabian passive margin. Within the limits of analytical uncertainty, the timing of eclogite-facies metamorphism in the Bitlis-Pütürge Massif and high-temperature, medium- to low-pressure metamorphism in the Akdağ metamorphic complex, the equivalent of Keban-Malatya metamorphic rocks (84–82 Ma vs. 83 ± 2 Ma, 2σ; early Campanian) are coeval (Oberhänsli et al., 2010, 2012, 2013; Rolland et al., 2012, 2020; Topuz et al., 2017). Accordingly, these two metamorphic belts may be interpreted as a paired metamorphic system (e.g., Brown, 2010; Miyashiro, 1973). The Bitlis-Pütürge Massif represents the subducted leading edge of the Arabian Platform, while the Keban-Malatya-Akdağ metamorphic rocks represent the high-temperature/middle-to low-pressure metamorphic rocks in the overriding plate, probably formed at the middle- to lower-crustal levels of a Late Cretaceous magmatic arc (Topuz et al., 2017). Amphibolite-facies retrogression in the Bitlis-Pütürge Massif occurred during the late Campanian to Maastrichtian, as indicated by Ar–Ar white mica ages of 74–69 Ma (Oberhänsli et al., 2010; Rolland et al., 2012). In contrast, the Akdağ metamorphic complex had already reached the Earth's surface by the late Campanian, as it is unconformably overlain by reefal limestone of Maastrichtian age (Topuz et al., 2017), a conclusion supported by the relatively rapid cooling of its Late Cretaceous intrusive rocks in the Baskil magmatic arc further south

10.1029/2025TC009243

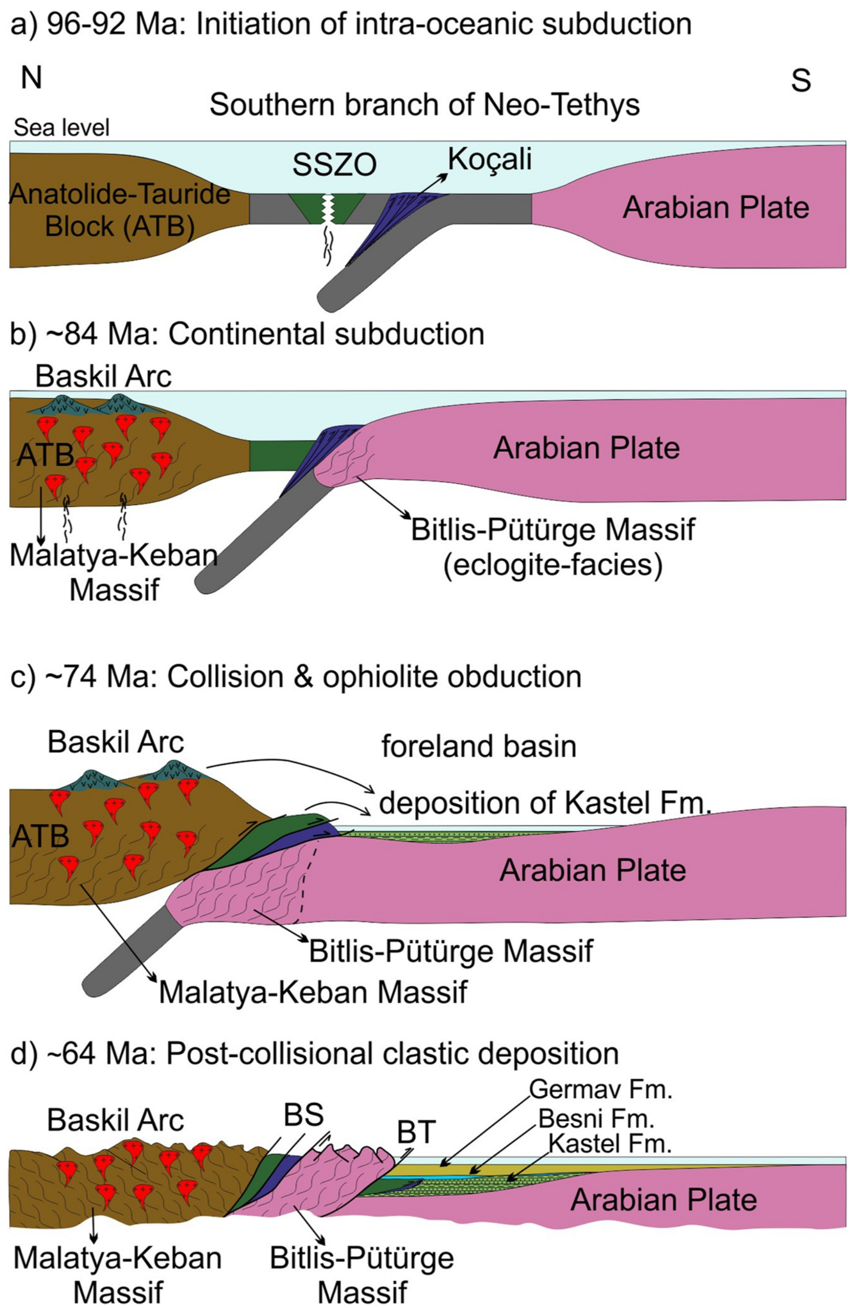

Figure 10. Schematic diagrams illustrating the tectonic evolution of the southern branch of the Neo-Tethys Ocean between the Anatolide-Tauride Block (Eastern Anatolia) and Arabian Plate in SE Türkiye (not to scale). (a) Inception of the convergence envisaged by the supra-subduction zone ophiolite (SSZO) formation. (b) Subduction of the leading edge of the Arabian Plate (continental subduction). (c) Derivation of active margin materials to the passive margin marking the collision onset, (d) post-collisional foreland deposition took place after exhumation of the Bitlis-Pütürge Massif, Malatya and Keban metamorphic rocks. BS, Bitlis Suture; BT, Bitlis Thrust.

(Karaoğlan et al., 2016). Thus, the exhumation of the two metamorphic belts occurred diachronously. This diachroneity in exhumation can be attributed to the mid-to late Campanian ophiolite emplacement onto the leading edge of the Arabian Platform, at a time when the Bitlis–Pütürge Massif remained at mid-crustal depths and underwent greenschist- to amphibolite-facies retrogression (Figure 10). This configuration is also reflected in the nature of the foreland deposits, as evidenced by the abundant occurrence of ophiolitic fragments in the Kastel Formation and the subsequent shift in detrital zircon age spectra observed in the Germav Formation, as discussed in the previous section. The timescale indicates that continental subduction preceded continental collision by ∼6–10 Myr. This temporal offset likely reflects the distance between the intraoceanic subduction zone and the Anatolide–Tauride Block, as a greater separation would prolong the interval between initial subduction of the Arabian margin and its eventual collision with the overriding plate. Such a configuration may explain why ophiolite emplacement and collision were nearly synchronous in SE Anatolia, in contrast to other orogenic belts where the subduction zone lay farther offshore. In summary, the above considerations indicate (a) continental subduction and eclogite-facies metamorphism at 84–82 Ma; (b) ophiolite obduction, continental collision, and retrograde evolution of the subducted continental margin at 74–69 Ma; and (c) exhumation of metamorphic units by 64 Ma, contemporaneous with deposition of the Germav Formation.

Assuming that the southern active margin of the Anatolide–Tauride Block evolved from oceanic subduction (ca. 96–82 Ma) to continental subduction (ca. 82–74 Ma), and ultimately to continental collision (beginning at ca. 74–71 Ma), a key question is whether Late Cretaceous magmatic rocks of the present-day East Anatolian Plateau recorded systematic compositional changes in response to these evolving tectonic regimes. Magmatism between 95 and 77 Ma is marked by tholeiitic affinity, juvenile isotopic compositions, and high-K calc-alkaline signatures, whereas magmatism from 77 to 69 Ma is dominated by nepheline-normative and shoshonitic compositions (Ersoy et al., 2024; Liu et al., 2022). Importantly, during continental subduction and the early phases of continental collision, magmatism became restricted to shoshonitic and nepheline-normative affinities. Furthermore, a pronounced magmatic lull (72–58 Ma; e.g., Schleiffarth et al., 2018) coincides with the initiation of continental collision, suggesting that collision-related geodynamic reorganization suppressed magma generation, marking a fundamental shift in the tectono-magmatic evolution of the Anatolide-Tauride Block. Thus, the hypothesis of an initial collision during the late Campanian is in line with a decrease in the amount of magmatism. Eocene magmatism is spatially restricted to a narrow zone within the Bitlis-Pütürge Massif, whereas voluminous Early Miocene to Quaternary magmatism extends across the entire East Anatolian Plateau and grades northward into the Pontides and eastward into the Lesser Caucasus. These contrasting spatial distributions imply distinct geodynamic drivers for the Eocene and Early Miocene to Quaternary magmatism. The spatially limited Eocene magmatism might be related to post-collisional events occurring along the suture zone (e.g., Ertürk et al., 2018), rather than to continental arc magmatism, while Early Miocene to Quaternary magmatism is better explained by crust–mantle interactions in a post-collisional setting, involving lithospheric peeling, dripping, or delamination that led to extreme thinning of the lithospheric mantle (e.g., Çubukçu et al., 2012; Keskin, 2003; Keskin et al., 1998; Özdemir & Güleç, 2014; Pearce et al., 1990; Schleiffarth et al., 2018; Topuz et al., 2019).

Paleomagnetic data from the crustal sections of suprasubduction zone ophiolites, such as Kızıldağ, Koçali, and Baer–Bassit that were obducted onto the Arabian Platform during middle to late Campanian, indicate formation at paleolatitudes of 21.4°N (+3.28/–2.94) and 20.6°N (±1.8; Morris, 2003; Cengiz et al., 2024). By comparison, Late Cretaceous volcanic rocks from the Sakarya Zone consistently yield higher paleolatitudes of 25–26°N (Channell et al., 1996; Meijers et al., 2010, 2011; Çinku Cengiz et al., 2017). Typical uncertainties in these paleolatitude estimates are on the order of ±5°, equivalent to ∼555 km (e.g., van Hinsbergen et al., 2020). Well-constrained paleomagnetic data from Upper Cretaceous sedimentary sequences in the Arabian Platform and Late Cretaceous igneous rocks in the Anatolide-Tauride Block remain absent. On the other hand, the amount of convergence between Eurasia and Arabia at the longitude of Türkiye is well-established from reconstructions of the Atlantic Ocean and the Red Sea, based on marine magnetic anomalies and fracture zones (e.g., Maffione et al., 2017; van Hinsbergen et al., 2024). For instance, for the location of the Kızıldağ Ophiolite, there was ∼2,300 km of Arabia-Eurasia convergence between 100 Ma and the present, and ∼1,900 km between 90 Ma and the present (see Figure 3 in van Hinsbergen et al., 2024). This convergence must have been accommodated by subduction along both the southern and northern branches of the Neo-Tethys Ocean, as well as by orogenic shortening along the northern margin of the Arabian Platform, the Pontides, and the intervening Anatolide–Tauride Block, as well as westward escape of Anatolia. Several studies indicate rapid convergence between the Arabian Platform and Eurasia at rates of ∼5–6 cm/a from 100 to 74 Ma, followed by slower convergence of ∼2–3 cm/a throughout the Cenozoic (e.g., Agard et al., 2011; McQuarrie & van Hinsbergen, 2013; Figure 3 in Boutoux et al., 2021). Subduction within the northern and southern Neo-Tethyan branches over 100–74 Ma (∼26 Ma at ∼5 cm/a) accounts for ∼1,300 km of convergence. Because closure of the northern Neo-Tethyan branch postdates that of the southern branch (ca. 65 Ma; e.g., Okay & Tüysüz, 1999; Okay et al., 2022; Topuz et al., 2011), only ∼180 km of the post-74 Ma convergence can be attributed to subduction within the northern Neo-Tethys. Thus, at least ∼1,480 km of the convergence was accommodated by oceanic subduction. Consistently, seismic tomography reveals a deep high-velocity anomaly at depths of ∼500–2,000 km within the lower mantle, which has been interpreted as a detached slab of the Neo-Tethyan ocean (Agard et al., 2011; Hafkenscheid et al., 2006; van der Meer et al., 2018). The remaining ∼820 km of post-collisional convergence may have been accommodated through a combination of shortening within the continental blocks located between Eurasia and the Arabian Platform (e.g., the Greater Caucasus, Bitlis–Pütürge Massif, Anatolide–Tauride Block, Pontides, Lesser Caucasus, and the Arabian Plate itself), together with closure of the Greater Caucasus Basin and westward extrusion of Anatolia (see Ballato et al., 2018, and references therein). Accordingly, estimates of post-Eocene convergence accommodated by shortening are on the order of ∼410 km in the Greater Caucasus, including closure of the Greater Caucasus Basin (Cowgill et al., 2016; van der Boon et al., 2018; van Hinsbergen et al., 2024), at least ∼350 km within the East Anatolian–Iranian Plateau (Agard et al., 2011; Boutoux et al., 2021; McQuarrie & van Hinsbergen, 2013; Pirouz et al., 2017), and ∼70 km through the westward extrusion of Anatolia (Ballato et al., 2018, and references therein). A detailed discussion of orogenic shortening in Eastern Anatolia and the Pontides is beyond the scope of this paper. However, the overall convergence budget and published shortening estimates can be broadly reconciled with a Campanian timing of collision along the Bitlis Suture, within the uncertainties inherent in both kinematic reconstructions and shortening estimates.

5.3. Comparison With Provenance Studies Along the Zagros Suture

A key question is whether continental closure along the Zagros Suture in Iran also occurred during the late Campanian, similar to that along the Bitlis Suture (Figure 1). Several provenance studies have been conducted on sedimentary successions within the foreland basin of the Arabian Platform, utilizing detrital zircon U–Pb–Hf isotopic data and heavy mineral assemblages (e.g., Cai et al., 2021; GholamiZadeh et al., 2022, 2025; Koshnaw et al., 2019, 2021; Sun et al., 2023; Zhang et al., 2017). These studies propose a wide range of timings for the onset of continental collision, ranging from earlier than 56 Ma (early Eocene) to as late as 10–5 Ma (Late Miocene-Pliocene). A common interpretation is that Paleocene and Eocene clastic sedimentary rocks were primarily sourced from obducted ophiolitic rocks, whereas Oligocene and Miocene sedimentary rocks were largely sourced from the Iranian Block north of the Zagros Suture. In this study, we re-evaluate the published detrital zircon age data from the Kermanshah and Khorramabad regions, which are presented in Figure 11 (Sun et al., 2023; Zhang et al., 2017). We present only the detrital zircon age spectra of biostratigraphically constrained Paleocene–Eocene clastic rocks because younger strata display similar age populations and do not record a distinguishable provenance shift.

Within the Iranian segment, the Amiran and Kashkan formations of the Kermanshah and Khorramabad regions are interpreted as eastward counterparts of the Kastel and Germav formations in southeastern Türkiye (Homke et al., 2009; Robertson et al., 2016). Biostratigraphy indicates that the Amiran Formation dates to the early Paleocene (64–61 Ma), whereas the Kashkan Formation is early Eocene (56–52 Ma) in the Kermanshah region (Sun et al., 2023). This suggests an age difference of ca. 10 Ma. Comparable to the Kastel Formation, the Amiran Formation contains abundant detritus sourced from obducted ophiolites (e.g., Sun et al., 2023). Paleocene clastic sedimentary rocks from the Kermanshah and Khorramabad areas contain a significant proportion of Jurassic zircons, along with additional age clusters between 105 and 92 Ma with εHf(t) values ranging from −5 to +10. Similarly, a common feature of the zircon age spectra of Eocene sandstones is the pronounced presence of Jurassic zircon grains, with peaks at 180 Ma and 170 Ma, closely correlating with the Sanandaj–Sirjan Zone to the north of the Zagros Suture. There is an ongoing debate regarding the origin of the extensive Middle Jurassic calc-alkaline magmatism in the Sanandaj–Sirjan Zone. Proposed interpretations include (a) a subduction-related setting (Esna-Ashari et al., 2016; Sarkarinejad et al., 2009; Sheikholeslami et al., 2008; Zhang et al., 2018) and (b) a rifting-related setting (Azizi & Stern, 2019; Stern et al., 2021). However, the local occurrence of Jurassic eclogites along the Zagros Suture (e.g., Montemagni et al., 2023; Wan et al., 2023) favors a subduction-related origin. In addition to the extensive Middle Jurassic magmatism in the Sanandaj–Sirjan Zone, a Late Jurassic oceanic arc—characterized by igneous zircon crystallization ages of 148–158 Ma—has been identified and is interpreted to have accreted during the Early Cretaceous (e.g., Azizi & Asahara, 2013; Azizi et al., 2015; Zarasvandi et al., 2015). Isotopically, these rocks exhibit relatively juvenile signatures, with initial εNd values ranging from +1.2 to +8. Notably, no Jurassic magmatism has been documented on the Arabian Platform. Therefore, Jurassic zircon grains found in Paleocene and Eocene clastic rocks on the Arabian Platform were likely derived either from the accreted Jurassic oceanic arc or from the continental arc of the Sanandaj–Sirjan Zone,

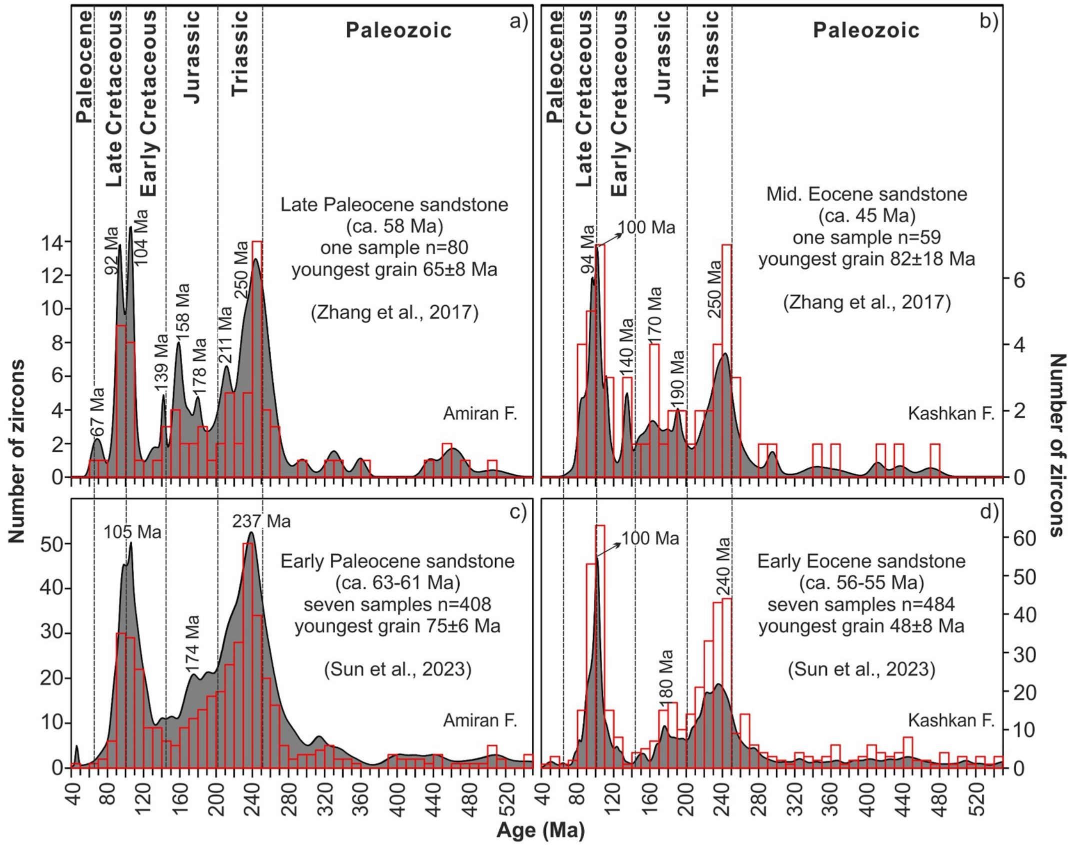

Figure 11. U–Pb detrital zircon age histograms with probability density curves for Paleocene and Eocene clastic rocks from the Arabian Foreland Basin to the south of the Zagros Suture. Bin width is set to 10 Ma. (a, b) Khorramabad region (Zhang et al., 2017), (c, d) the Kermanshah area (Sun et al., 2023). For the locations of Khorramabad and Kermanshah areas, see Figures 1 and 12b.

located north of the Zagros Suture. However, the wide range of detrital zircon ages (190–140 Ma), together with the presence of numerous grains exhibiting negative initial εHf values, suggests that the Sanandaj–Sirjan Zone was the most likely dominant provenance. Based on the detrital zircon record from Paleocene–Eocene clastic successions, we infer that continental collision in the Kermanshah and Khorramabad areas occurred during Maastrichtian-early Paleocene, coinciding with the onset of deposition of the Amiran Formation (Sun et al., 2023).

Late Cretaceous supra-subduction zone ophiolites and related ophiolitic mélanges are exposed in areas such as Kermanshah, Neyriz, and Hajiabad, which are interpreted to have been obducted over the leading edge of the Arabian Platform during middle Campanian-early Maastrichtian, similar to the Kızıldağ and Guleman ophiolites in Türkiye (Babaie et al., 2006; Moghadam et al., 2022; Moghadam & Stern, 2015). Their formation ages were determined as 96–100 Ma by U–Pb zircon dating, slightly older than Kızıldağ, Koçali, and Troodos. The zircon εHf(t) values range from +9 to +26 (Moghadam et al., 2022). High-pressure metamorphic rocks, such as blueschists with $^{40}Ar/^{39}Ar$ phengite ages of 95–85 Ma, have only been documented from the Hajiabad area (Agard et al., 2006). In the Kermanshah area, Eocene metamorphic and volcanosedimentary rocks, interpreted as ophiolitic rocks, have been reported (Ao et al., 2016; Moghadam & Stern, 2015); however, the nature of these occurrences remains uncertain, as several samples contain a high proportion of inherited zircon xenocrysts with ages ranging from 140 to 2,150 Ma.

5.4. Geodynamic Implications

Widely used paleogeographic reconstructions propose a major transform fault between Eastern Anatolia and the NW Iranian Block (e.g., Barrier & Vrielynck, 2008; Stampfli & Borel, 2002; van Hinsbergen et al., 2020), largely

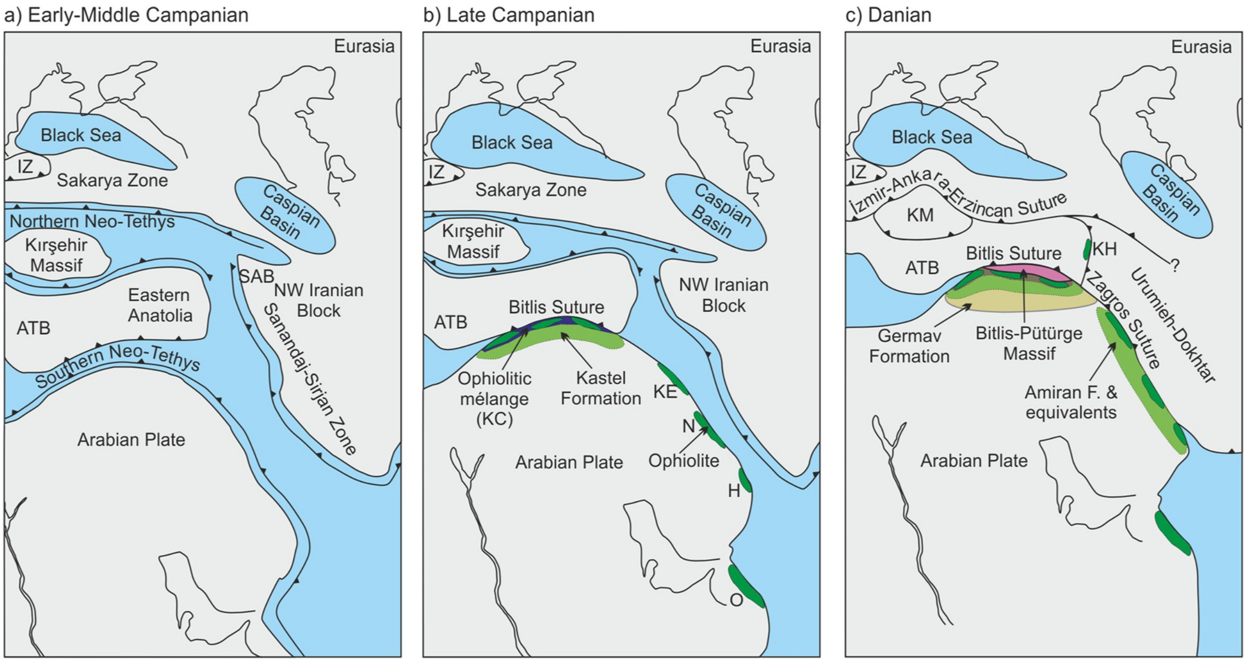

Figure 12. Paleogeographic sketch maps modified from Barrier et al. (2018) for pre-collisional (a), collisional (b) and post-collisional stages (c). IZ, İstanbul Zone, ATB, Anatolide-Tauride Block; KM, Kırşehir Massif; KC, Koçali Complex; KE, Kermanshah Ophiolite; KH, Khoy Ophiolite; N, Neyriz Ophiolite; O, Oman Ophiolite; H, Hajiabad Ophiolite; SAB, South Armenian Block.

because the northern Neo-Tethys can be traced into Armenia and Karabagh but not farther into northern Iran (Figure 1). The NW Iranian Block is interpreted to have accreted northward during the latest Triassic, and the suture parallel to the Alborz Mountains toward Mashhad is therefore commonly regarded as the Paleo-Tethyan Suture (e.g., Berberian & King, 1981; Şengör, 1990). There are several notable geological differences between Eastern Anatolia and the NW Iranian Block. These include (a) the absence of any equivalent to the Bitlis–Pütürge Massif in Iran, which represents the subducted northern margin of the Arabian Platform, (b) the absence of Jurassic magmatism north of the Bitlis Suture, in contrast to its widespread presence in Iran, particularly in the Sanandaj–Sirjan Zone north of the Zagros Suture, as well as the local occurrence of Jurassic eclogites along the Zagros Suture (e.g., Montemagni et al., 2023; Wan et al., 2023), (c) the rarity of Late Cretaceous arc-related igneous rocks north of the Zagros Suture, compared to their widespread occurrence in Eastern Anatolia (e.g., Ertürk et al., 2022; Karaoğlan et al., 2016; Lechmann et al., 2018; Liu et al., 2022; Rızaoğlu et al., 2006; Sar et al., 2019; Ural et al., 2021), (d) widespread Late Cretaceous high-temperature/medium- to low-pressure metamorphism in Eastern Anatolia (Topuz et al., 2017), and its absence in the NW Iranian Block, and (e) the development of a linear Eocene–Oligocene magmatic belt in Iran (Urumieh-Dokhtar magmatic belt). This magmatic belt is approximately 50–60 km wide and is located ∼150–200 km north of the Zagros Suture, extending for >1,750 km parallel to it. In contrast, Eocene volcanic rocks in the Turkish segment are minor and restricted to the suture zone and the Bitlis–Pütürge Massif, although they may grade northward into Eocene magmatism in the Sakarya Zone of northern Türkiye (Figure 12; Berberian & King, 1981; Ertürk et al., 2018; Mohamadi Chaghamarani et al., 2025; Okay et al., 2022; Şengör, 1990; Stern et al., 2021; Verdel et al., 2011 for Eocene magmatism in Iran). The widespread Eocene magmatism along the Urumieh–Dokhtar magmatic belt has been interpreted either as arc-related, reflecting ongoing Neo-Tethyan subduction (e.g., Rabiee et al., 2022; Stern et al., 2021; Verdel et al., 2011), or alternatively as post-collisional (e.g., Ghasemi & Talbot, 2006; Mazhari et al., 2009). We infer that this contrast reflects the fact that Eastern Anatolia and the NW Iranian Block represent distinct continental blocks separated by the Azerbaijan Neo-Tethyan Suture. Thus, within the tectonic framework proposed in this study, the nature of the Eocene magmatism may require reassessment of the currently available geochemical data. Ophiolites and ophiolitic mélanges occur along the Azerbaijan Suture, delineating the boundary between Eastern Anatolia and the NW Iranian Block. The largest of these is the Khoy ophiolite (Figure 1). Geological and geochronological data indicate that the Khoy region comprises multiple meta-igneous complexes of distinct ages, including Ediacaran–Cambrian (ca. 606–517 Ma) and Jurassic (ca. 160 Ma) units, comparable to magmatic ages reported from the Sanandaj–Sirjan Zone. These are accompanied by a younger, non-metamorphic ophiolitic complex of Late Cretaceous age (e.g., Azizi et al., 2011; Khalatbari-Jafari et al., 2004; Moghadam et al., 2019). Khalatbari-Jafari et al. (2004) suggested a latest Cretaceous–earliest Paleocene age for emplacement of the Khoy ophiolite, immediately preceding continental collision.

The tectonic affinity of the South Armenian Block also remains debated. It has been interpreted as the easternmost extension of the Anatolide–Tauride Block (Rolland et al., 2020) or as an isolated microplate (Braitenberg et al., 2025; van Hinsbergen et al., 2020). Following Mohamadi Chaghamarani et al. (2025), we instead interpret the South Armenian Block as the western continuation of the NW Iranian Block, based on pronounced stratigraphic contrasts with Eastern Anatolia; the South Armenian Block contains Jurassic volcanogenic sedimentary rocks intruded by Late Jurassic to Early Cretaceous granitoids, whereas the Anatolide–Tauride Block lacks evidence of Jurassic and Early Cretaceous magmatism and metamorphism (e.g., Hässig et al., 2015, 2020; Topuz et al., 2017). Consistent with Şengör (1990) and Topuz et al. (2017), we infer the existence of a Neo-Tethyan Suture (the Azerbaijan Suture) linking the İzmir–Ankara–Erzincan and Zagros Neo-Tethyan sutures. Within this framework, closure of the İzmir–Ankara–Erzincan, Azerbaijan, and Zagros Neo-Tethyan oceanic domains was broadly synchronous and was likely remained open after closure of the southern Neo-Tethys Ocean along the Bitlis Suture in the late Campanian, and were subsequently consumed within the same subduction system (Figure 12; modified from Barrier et al., 2018). This configuration provides a first-order explanation for the marked geological differences between Eastern Anatolia and the NW Iranian Block.

To sum up, closure of the southern Neo-Tethys was diachronous, with continental collision initiating in southeastern Türkiye during the late Campanian and progressing eastward to the Kermanshah and Khorramabad regions during the Maastrichtian-early Paleocene, spanning up to ~10 Myr. In contrast, closure of the northern Neo-Tethys occurred later, during the Paleocene to early Eocene(?), along the İzmir–Ankara–Erzincan Suture (Okay, Sunal, et al., 2020; Okay & Tüysüz, 1999) and the Azerbaijan Suture, broadly coinciding with the timing of final closure of the southern Neo-Tethys along the Zagros Suture in the Kermanshah and Khorramabad areas. This diachronous tectonic evolution carries important geodynamic implications, indicating that the Bitlis Suture cannot be interpreted simply as the site of a direct Eurasia–Arabia collision. At the time of closure of the Bitlis Suture, the Eastern Anatolian continental block (Anatolide–Tauride Block) had not yet accreted to the Pontides (Eurasia).

6. Conclusions

Integrated biostratigraphic, petrographic, and geochronological data from Upper Campanian clastic deposits in the Adıyaman sector of the Arabian Foreland Basin show that these strata are overwhelmingly dominated by Late Cretaceous zircons (100–83 Ma) with arc-like isotopic signatures, together with abundant ophiolitic lithic fragments. The absence of coeval magmatism on the Arabian Plate precludes a southern source and instead indicates sediment supply from a magmatic arc north of the Bitlis Suture, as well as from obducted ophiolitic rocks. This implies that the northwestern margin of the Arabian Plate had already collided with Eastern Anatolia by ~74–71 Ma (late Campanian). In contrast, Danian strata record a clear provenance shift along the Arabian margin, marked by a broader zircon age spectrum that includes a substantial proportion of Cambrian and Proterozoic zircons in addition to Late Cretaceous–early Paleocene grains. This shift likely reflects exhumation of the Bitlis–Pütürge Massif, which contains abundant late Neoproterozoic–Cambrian igneous rocks, together with exhumation of the middle to lower crustal levels of the Late Cretaceous Baskil magmatic arc by the early Paleocene.

The timing of ophiolite obduction onto the leading margin of the Arabian Platform and the inferred onset of continental collision do not differ significantly, thereby challenging tectonic models that depict the Bitlis–Pütürge Massif as an isolated continental block flanked by subduction zones to the north and south, which are proposed to have closed during the Late Cretaceous and Miocene, respectively. The coeval occurrence of high-pressure metamorphism in the Bitlis–Pütürge Massif and high-temperature metamorphism in the Malatya–Keban–Akdağ massifs, which form the basement of Eastern Anatolia, suggests the presence of a paired metamorphic belt system. Late Cretaceous basic to acidic magmatism in Eastern Anatolia represents arc-related magmatism. However, the onset of continental collision led to a magmatic lull. Both the spatially limited Eocene magmatism and the voluminous Neogene to Quaternary magmatism represent episodes of post-collisional magmatic activity. The younger low-temperature thermochronological data from the Bitlis–Pütürge Massif, previously attributed to the timing of continental collision, and from the East Anatolian Plateau might reflect punctuated episodes of increased intraplate deformation in the context of sustained convergence between the Arabian Platform and Eurasia since the Late Cretaceous.

A critical reappraisal of detrital zircon U–Pb age data from the Iranian segment of the Arabian Foreland Basin suggests that collision occurred somewhat later, during the Maastrichtian-early Palocene in the Kermanshah and Khorramabad areas. This timing predates most previously proposed estimates for the onset of collision in southeastern Türkiye and Iran. Thus, closure of the southern Neo-Tethys along the Bitlis Suture preceded that along the İzmir–Ankara–Erzincan Suture, with final suturing between Eurasia and Arabia achieved along the İzmir–Ankara–Erzincan, Zagros, and Azerbaijan Neo-Tethyan sutures. This tectonic configuration provides a coherent explanation for the pronounced Mesozoic and early Cenozoic geological differences between Eastern Anatolia and the NW Iranian block. Consequently, a refinement of existing regional tectonic models is required.

Conflict of Interest

The authors declare no conflicts of interest relevant to this study.

Availability Statement

All new data presented in this article are available in the Supporting Information File (SI, Text "Analytical Procedures", Figures S1–S6 in Supporting Information S1 and Tables S1–S7), and can be downloaded from a Zenodo repository (https://zenodo.org/records/20871318).

Acknowledgments
We gratefully acknowledge the editorial handling by Taylor Schildgen and the constructive and insightful reviews provided by Paolo Ballato (Associate Editor), William Cavazza, Nurettin Kaymakçı, and two anonymous reviewers. This study was financially supported by the National Science Foundation of China–Tethyan Major Project (Grant 91755209) and the İstanbul Technical University BAP Project (MAB-2024-45589). We have greatly benefited from discussions with Douwe J.J. van Hinsbergen on paleomagnetism and the amount of convergence in Eastern Anatolia. We thank Boris Natal'in and Mehmet Keskin for their assistance in constructing the crustal-scale cross section across Eastern Anatolia; Tuna Eken for preparing the relief map; Ali Yetgin Egi, Ali Fırat, and Lai Wen for their help during fieldwork; Wei Li for support with U–Pb zircon dating; and Evren Çubukçu for cathodoluminescence (CL) imaging of zircon grains.

References

Açlan, M., & Altun, Y. (2018). Syn-collisional I-type Esenköy Pluton (Eastern Anatolia-Turkey): An indication for collision between Arabian and Eurasian plates. *Journal of African Earth Sciences*, *142*, 1–11. https://doi.org/10.1016/j.jafrearsci.2018.02.019

Agard, P., Monié, P., Gerber, W., Omrani, J., Molinaro, M., Meyer, B., et al. (2006). Transient, synobduction exhumation of Zagros blueschists inferred from P-T, deformation, time, and kinematic constraints: Implications for Neotethyan wedge dynamics. *Journal of Geophysical Research*, *111*(B11). https://doi.org/10.1029/2005JB004103

Agard, P., Omrani, J., Jolivet, L., Whitechurch, H., Vrielynck, B., Spakman, W., et al. (2011). Zagros orogeny: A subduction-dominated process. *Geological Magazine*, *148*(5–6), 692–725. https://doi.org/10.1017/S001675681100046X

Agnini, C., Fornaciari, E., Raffi, I., Catanzariti, R., Pälike, H., Backman, J., & Rio, D. (2014). Biozonation and biochronology of Paleogene calcareous nannofossils from low and middle latitudes. *Newsletters on stratigraphy*, *47*(2), 131–181. https://doi.org/10.1127/0078-0421/2014/0042

Akdoğan, R., Hu, X., Okay, A. I., Topuz, G., & Xue, W. (2021). Provenance of the Paleozoic to Mesozoic siliciclastic rocks of the Istanbul Zone constrains the timing of the Rheic Ocean closure in the Eastern Mediterranean region. *Tectonics*, *40*(12), e2021TC006824. https://doi.org/10.1029/2021TC006824

Alavi, M. (1994). Tectonics of the Zagros orogenic belt of Iran: New data and interpretations. *Tectonophysics*, *229*(3–4), 211–238. https://doi.org/10.1016/0040-1951(94)90030-2

Albino, I., Cavazza, W., Zattin, M., Okay, A. I., Adamia, S., & Sadradze, N. (2014). Far-field tectonic effects of the Arabia–Eurasia collision and the inception of the North Anatolian Fault system. *Geological Magazine*, *151*(2), 372–379. https://doi.org/10.1017/S0016756813000952

Ao, S., Xiao, W., Jafari, M. K., Talebian, M., Chen, L., Wan, B., et al. (2016). U–Pb zircon ages, field geology and geochemistry of the Kermanshah ophiolite (Iran): From continental rifting at 79 Ma to oceanic core complex at ca. 36 Ma in the southern Neo-Tethys. *Gondwana Research*, *31*, 305–318. https://doi.org/10.1016/j.gr.2015.01.014

Azizi, H., & Asahara, Y. (2013). Juvenile granite in the Sanandaj–Sirjan Zone, NW Iran: Late Jurassic–early Cretaceous arc–continent collision. *International Geology Review*, *55*(12), 1523–1540. https://doi.org/10.1080/00206814.2013.782959

Azizi, H., Chung, S. L., Tanaka, T., & Asahara, Y. (2011). Isotopic dating of the Khoy metamorphic complex (KMC), northwestern Iran: A significant revision of the formation age and magma source. *Precambrian Research*, *185*(3–4), 87–94. https://doi.org/10.1016/j.precamres.2010.12.004

Azizi, H., Najari, M., Asahara, Y., Catlos, E. J., Shimizu, M., & Yamamoto, K. (2015). U–Pb zircon ages and geochemistry of Kangareh and Taghiabad mafic bodies in northern Sanandaj–Sirjan Zone, Iran: Evidence for intra-oceanic arc and back-arc tectonic regime in late Jurassic. *Tectonophysics*, *660*, 47–64. https://doi.org/10.1016/j.tecto.2015.08.008

Azizi, H., & Stern, R. J. (2019). Jurassic igneous rocks of the central Sanandaj–Sirjan zone (Iran) mark a propagating continental rift, not a magmatic arc. *Terra Nova*, *31*(5), 415–423. https://doi.org/10.1111/ter.12404

Babaie, H. A., Babaei, A., Ghazi, A. M., & Arvin, M. (2006). Geochemical, 40Ar/39Ar age, and isotopic data for crustal rocks of the Neyriz ophiolite, Iran. *Canadian Journal of Earth Sciences*, *43*(1), 57–70. https://doi.org/10.1139/e05-111

Backman, J., & Shackleton, N. J. (1983). Quantitative biochronology of Pliocene and early Pleistocene calcareous nannofossils from the Atlantic, Indian and Pacific oceans. *Marine Micropaleontology*, *8*(2), 141–170. https://doi.org/10.1016/0377-8398(83)90009-9

Ballato, P., Parra, M., Schildgen, T. F., Dunkl, I., Yıldırım, C., Özsayın, E., et al. (2018). Multiple exhumation phases in the Central Pontides (N Turkey): New temporal constraints on major geodynamic changes associated with the closure of the Neo-Tethys Ocean. *Tectonics*, *37*(6), 1831–1857. https://doi.org/10.1029/2017TC004808

Ballato, P., Uba, C. E., Landgraf, A., Strecker, M. R., Sudo, M., Stockli, D. F., et al. (2011). Arabia-Eurasia continental collision: Insights from late Tertiary foreland-basin evolution in the Alborz Mountains, northern Iran. *GSA Bulletin*, *123*(1–2), 106–131. https://doi.org/10.1130/B30091.1

Barrier, E., & Vrielynck, B. (2008). *MEBE Atlas - Paleotectonic maps of the Middle East. Tectono-Sedimentary-Palinspatic maps from late Norian to Plieocene*. Commission for the Geological Map of the World. Retrieved from https://ccgm.org/en/product/atlas-of-paleotectonicmaps-of-the-middle-east-mebe-program

Barrier, E., Vrielynck, B., Brouillet, J. F., & Brunet, M. F. (2018). *Paleotectonic reconstruction of the Central Tethyan Realm. Tectonono-sedimentary-palinspastic maps from late Permian to Pliocene*. Commission for the Geological Map of the World. Retrieved from https://www.ccgm.org/en/product/darius-atlas-pdf/

Belousova, E. A., Griffin, W. L., O'Reilly, S. Y., & Fisher, N. L. (2002). Igneous zircon: Trace element composition as an indicator of source rock type. *Contributions to Mineralogy and Petrology*, *143*(5), 602–622. https://doi.org/10.1007/s00410-002-0364-7

Berberian, M., & King, G. C. P. (1981). Towards a paleogeography and tectonic evolution of Iran. *Canadian Journal of Earth Sciences*, *18*(2), 210–265. https://doi.org/10.1139/e81-019

Beyarslan, M., & Bingöl, A. F. (2018). Zircon U-Pb age and geochemical constraints on the origin and tectonic implications of late Cretaceous intra-oceanic arc magmatics in the Southeast Anatolian Orogenic Belt (SE-Turkey). *Journal of African Earth Sciences*, *147*, 477–497. https://doi.org/10.1016/j.jafrearsci.2018.07.001

Beyarslan, M., Lin, Y. C., Bingöl, A. F., & Chung, S. L. (2016). Zircon U-Pb age and geochemical constraints on the origin and tectonic implication of Cadomian (Ediacaran-Early Cambrian) magmatism in SE Turkey. *Journal of Asian Earth Sciences*, *130*, 223–238. https://doi.org/10.1016/j.jseaes.2016.08.006

Bingöl, A. F., Beyarslan, M., Lin, Y. C., & Lee, H. Y. (2018). Geochronological and geochemical constraints on the origin of the Southeast Anatolian ophiolites, Turkey. *Arabian Journal of Geosciences*, *11*(18), 1–40. https://doi.org/10.1007/s12517-018-3880-0

Boutoux, A., Briaud, A., Faccenna, C., Ballato, P., Rossetti, F., & Blanc, E. (2021). Slab folding and surface deformation of the Iran mobile belt. *Tectonics*, *40*(6), e2020TC006300. https://doi.org/10.1029/2020TC006300

Braitenberg, C., Maurizio, G., Pivetta, T., Pastorutti, A., & Cavazza, W. (2025). Satellite gravity fields and the identification of accreted microplates. *Geoscience Frontiers*, *16*(2), 101976. https://doi.org/10.1016/j.gsf.2024.101976

Brown, M. (2010). Paired metamorphic belts revisited. *Gondwana Research*, *18*(1), 46–59. https://doi.org/10.1016/j.gr.2009.11.004

Burg, J. P. (2018). Geology of the onshore Makran accretionary wedge: Synthesis and tectonic interpretation. *Earth-Science Reviews*, *185*, 1210–1231. https://doi.org/10.1016/j.earscirev.2018.09.011

Cai, F., Ding, L., Wang, H., Laskowski, A. K., Zhang, L., Zhang, B., et al. (2021). Configuration and timing of collision between Arabia and Eurasia in the Zagros collision zone, Fars, southern Iran. *Tectonics*, *40*(8), e2021TC006762. https://doi.org/10.1029/2021TC006762

Cavazza, W., Cattò, S., Zattin, M., Okay, A. I., & Reiners, P. (2018). Thermochronology of the Miocene Arabia-Eurasia collision zone of southeastern Turkey. *Geosphere*, *14*(5), 2277–2293. https://doi.org/10.1130/GES01637.1

Cawood, P. A., Hawkesworth, C. J., & Dhuime, B. (2012). Detrital zircon record and tectonic setting. *Geology*, *40*(10), 875–878. https://doi.org/10.1130/G32945.1

Cengiz, M., Karabulut, S., Çabuk, B. S., & Rajtschan, V. (2024). Paleomagnetic data bearing on the origin of the supra-subduction zone ophiolites in southeast Anatolia and the progressive closure of the Neotethys Ocean in the Eastern Mediterranean. *Tectonics*, *43*(11), e2024TC008386. https://doi.org/10.1029/2024TC008386

Channell, J. E. T., Tüysüz, O., Bektas, O., & Sengör, A. M. C. (1996). Jurassic-Cretaceous paleomagnetism and paleogeography of the Pontides (Turkey). *Tectonics*, *15*(1), 201–212. https://doi.org/10.1029/95TC02290

Çinku Cengiz, M., Heller, F., & Ustaömer, T. (2017). New paleomagnetic results from Upper Cretaceous arc-type rocks from the northern and southern branches of the Neotethys ocean in Anatolia. *International Journal of Earth Sciences*, *106*(7), 2575–2592. https://doi.org/10.1007/s00531-017-1447-z

Cohen, K. M., Harper, D., Gibbard, P., & Car, N. (2025). The ICS international chronostratigraphic chart. *Episodes*, *48*(1), 105–115. https://doi.org/10.18814/epiiugs/2025/025001

Cowgill, E., Forte, A. M., Niemi, N., Avdeev, B., Tye, A., Trexler, C., et al. (2016). Relict basin closure and crustal shortening budgets during continental collision: An example from Caucasus sediment provenance. *Tectonics*, *35*(12), 2918–2947. https://doi.org/10.1002/2016TC004295

Çubukçu, H. E., Ulusoy, I., Aydar, E., Ersoy, O., Şen, E., Gourgaud, A., & Guillou, H. (2012). Mt. Nemrut volcano (Eastern Turkey): Temporal petrological evolution. *Journal of Volcanology and Geothermal Research*, *209*, 33–60. https://doi.org/10.1016/j.jvolgeores.2011.08.005

Darin, M. H., & Umhoefer, P. J. (2022). Diachronous initiation of Arabia–Eurasia collision from eastern Anatolia to the southeastern Zagros Mountains since middle Eocene time. *International Geology Review*, *64*(18), 2653–2681. https://doi.org/10.1080/00206814.2022.2048272

Darin, M. H., Umhoefer, P. J., & Thomson, S. N. (2018). Rapid late Eocene exhumation of the Sivas Basin (Central Anatolia) driven by initial Arabia-Eurasia collision. *Tectonics*, *37*(10), 3805–3833. https://doi.org/10.1029/2017TC004954

Dickinson, W. R. (1970). Interpreting detrital modes of graywacke and arkose. *Journal of Sedimentary Research*, *40*(2), 695–707. https://doi.org/10.1306/74d72018-2b21-11d7-8648000102c1865d

Dickinson, W. R., Beard, L. S., Brakenridge, G. R., Erjavec, J. L., Ferguson, R. C., Inman, K. F., et al. (1983). Provenance of North American Phanerozoic sandstones in relation to tectonic setting. *Geological Society of America Bulletin*, *94*(2), 222–235. https://doi.org/10.1130/0016-7606(1983)94<222:PONAPS>2.0.CO;2

Dickinson, W. R., & Gehrels, G. E. (2009). Use of U–Pb ages of detrital zircons to infer maximum depositional ages of strata: A test against a Colorado Plateau Mesozoic database. *Earth and Planetary Science Letters*, *288*(1–2), 115–125. https://doi.org/10.1016/j.epsl.2009.09.013

Dilek, Y., & Thy, P. (2009). Island arc tholeiite to boninitic melt evolution of the Cretaceous Kizildag (Turkey) ophiolite: Model for multi-stage early arc–forearc magmatism in Tethyan subduction factories. *Lithos*, *113*(1–2), 68–87. https://doi.org/10.1016/j.lithos.2009.05.044

Duran, O., Şemşir, D., Sezgin, İ., & Perinçek, D. (1988). *Stratigraphy, sedimentology of the Midyat and Silvan Groups and their hydrocarbon potentials, southeast Turkey* (Vol. 1, pp. 99–126). Türkiye Petrol Jeologları Derneği Bülteni.

Eken, T., Tork, Q. M., Schiffer, C., Taymaz, T., & Saygın, E. (2021). New insights into crustal properties of Anatolia and its surroundings inferred from P-Coda autocorrelation inversions. *Journal of Geophysical Research: Solid Earth*, *126*(12), e2021JB023184. https://doi.org/10.1029/2021JB023184

Ersoy, Y. E., Uysal, İ., Candan, O., Palmer, M. R., & Müller, D. (2024). Petrogenesis of late Campanian Alkaline Igneous Rocks in Eastern Anatolia: Magmatism related to a subduction transform edge propagator (STEP) fault? *International Geology Review*, *66*(2), 533–555. https://doi.org/10.1080/00206814.2023.2201830

Ertürk, M. A. (2025). Geochronology and petrology of Late Cretaceous subduction-related volcanics from Elazığ, SE Türkiye: Insights into deciphering petrogenesis and magma generation processes. *Geochemistry*, *85*(1), 126234. https://doi.org/10.1016/j.chemer.2024.126234

Ertürk, M. A., Beyarslan, M., Chung, S. L., & Lin, T. H. (2018). Eocene magmatism (Maden Complex) in the Southeast Anatolian orogenic belt: Magma genesis and tectonic implications. *Geoscience Frontiers*, *9*(6), 1829–1847. https://doi.org/10.1016/j.gsf.2017.09.008

Ertürk, M. A., Sar, A., & Rizeli, M. E. (2022). Petrology, zircon U–Pb geochronology and tectonic implications of the A1-type intrusions: Keban region, eastern Turkey. *Geochemistry*, *82*(3), 125882. https://doi.org/10.1016/j.chemer.2022.125882

Esna-Ashari, A., Tiepolo, M., & Hassanzadeh, J. (2016). On the occurrence and implications of Jurassic primary continental boninite-like melts in the Zagros orogen. *Lithos*, *258*, 37–57. https://doi.org/10.1016/j.lithos.2016.04.017

Ewing, T. A., & Müntener, O. (2018). The mantle source of island arc magmatism during early subduction: Evidence from Hf isotopes in rutile from the Jijal Complex (Kohistan arc, Pakistan). *Lithos*, *308*, 262–277. https://doi.org/10.1016/j.lithos.2018.03.005

Eyüboğlu, Y., Dudas, F. O., Zhu, D. C., Liu, Z., & Chatterjee, N. (2019). Late Cretaceous I-and A-type magmas in eastern Turkey: Magmatic response to double-sided subduction of Paleo-and Neo-Tethyan lithospheres. *Lithos*, *326*, 39–70. https://doi.org/10.1016/j.lithos.2018.12.017

Faccenna, C., Bellier, O., Martinod, J., Piromallo, C., & Regard, V. (2006). Slab detachment beneath eastern Anatolia: A possible cause for the formation of the North Anatolian fault. *Earth and Planetary Science Letters*, *242*(1–2), 85–97. https://doi.org/10.1016/j.epsl.2005.11.046

Gardin, S., Galbrun, B., Thibault, N., Coccioni, R., & Silva, I. P. (2012). Bio-magnetochronology for the upper Campanian-Maastrichtian from the Gubbio area, Italy: New results from the Contessa Highway and Bottaccione sections. *Newsletters on Stratigraphy*, *45*(1), 75–103. https://doi.org/10.1127/0078-0421/2012/0014

Garzanti, E. (2019). The Himalayan Foreland Basin from collision onset to the present: A sedimentary–petrology perspective. *Geological Society, London, Special Publications*, *483*(1), 65–122. https://doi.org/10.1144/SP483.17

GEBCO Bathymetric Compilation Group. (2019). *The GEBCO_2019 Grid—A continuous terrain model of the global oceans and land*. British Oceanographic Data Centre, National Oceanography Centre. https://doi.org/10.5285/836f016a-33be-6ddc-e053-6c86abc0788e

Gehrels, G. (2014). Detrital zircon U-Pb geochronology applied to tectonics. *Annual Review of Earth and Planetary Sciences*, *42*(1), 127–149. https://doi.org/10.1146/annurev-earth-050212-124012

Ghasemi, A., & Talbot, C. J. (2006). A new tectonic scenario for the Sanandaj–Sirjan Zone (Iran). *Journal of Asian Earth Sciences*, *26*(6), 683–693. https://doi.org/10.1016/j.jseaes.2005.01.003

GholamiZadeh, P., Hu, X., Garzanti, E., & Adabi, M. H. (2022). Constraining the timing of Arabia-Eurasia collision in the Zagros orogen by sandstone provenance (Neyriz, Iran). *Geological Society of America Bulletin*, *134*(7–8), 1793–1810. https://doi.org/10.1130/B35950.1

GholamiZadeh, P., Wan, B., Garzanti, E., Hu, X., Esmaeili, R., & Ebrahimi, M. (2025). Collision timing and provenance shifts from the late Oligocene to Middle Miocene in the southeasternmost Zagros orogen. *Scientific Reports*, *15*(1), 6023. https://doi.org/10.1038/s41598-025-90186-x

Gradstein, F., Ogg, J. G., Schmitz, M. D., & Ogg, G. M. (2012). *The geologic time scale 2012*. Elsevier.1176.

Grimes, C. B., Wooden, J. L., Cheadle, M. J., & John, B. E. (2015). "Fingerprinting" tectono-magmatic provenance using trace elements in igneous zircon. *Contributions to Mineralogy and Petrology*, *170*(5–6), 1–26. https://doi.org/10.1007/s00410-015-1199-3

Gün, E., Pysklywec, R. N., Göğüş, O. H., & Topuz, G. (2021). Pre-collisional extension of microcontinental terranes by a subduction pulley. *Nature Geoscience*, *14*(6), 443–450. https://doi.org/10.1038/s41561-021-00746-9

Gürsu, S., Moeller, A., Göncüoglu, M. C., Köksal, S., Demircan, H., Köksal, F. T., et al. (2015). Neoproterozoic continental arc volcanism at the northern edge of the Arabian Plate, SE Turkey. *Precambrian Research*, *258*, 208–233. https://doi.org/10.1016/j.precamres.2014.12.017

Hafkenscheid, E., Wortel, M. J. R., & Spakman, W. (2006). Subduction history of the Tethyan region derived from seismic tomography and tectonic reconstructions. *Journal of Geophysical Research*, *111*(B8). https://doi.org/10.1029/2005JB003791

Haq, B. U. (2014). Cretaceous eustasy revisited. *Global and Planetary Change*, *113*, 44–58. https://doi.org/10.1016/j.gloplacha.2013.12.007

Hässig, M., Moritz, R., Ulianov, A., Popkhadze, N., Galoyan, G., & Enukidze, O. (2020). Jurassic to Cenozoic magmatic and geodynamic evolution of the Eastern Pontides and Caucasus belts, and their relationship with the Eastern Black Sea Basin opening. *Tectonics*, *39*(10), e2020TC006336. https://doi.org/10.1029/2020TC006336

Hässig, M., Rolland, Y., Sahakyan, L., Sosson, M., Galoyan, G., Avagyan, A., et al. (2015). Multi-stage metamorphism in the South Armenian Block during the late Jurassic to Early Cretaceous: Tectonics over south-dipping subduction of Northern branch of Neotethys. *Journal of Asian Earth Sciences*, *102*, 4–23. https://doi.org/10.1016/j.jseaes.2014.07.018

Hempton, M. R. (1985). Structure and deformation history of the Bitlis suture near Lake Hazar, southeastern Turkey. *Geological Society of America Bulletin*, *96*(2), 233–243. https://doi.org/10.1130/0016-7606(1985)96<233:SADHOT>2.0.CO;2

Homke, S., Vergés, J., Serra-Kiel, J., Bernaola, G., Sharp, I., Garcés, M., et al. (2009). Late Cretaceous–Paleocene formation of the proto–zagros foreland basin, Lurestan Province, SW Iran. *Geological Society of America Bulletin*, *121*(7–8), 963–978. https://doi.org/10.1130/B26035.1

Hoskin, P. W., & Ireland, T. R. (2000). Rare earth element chemistry of zircon and its use as a provenance indicator. *Geology*, *28*(7), 627–630. https://doi.org/10.1130/0091-7613(2000)28<627:REECOZ>2.0.CO;2

Hoskin, P. W., & Schaltegger, U. (2003). The composition of zircon and igneous and metamorphic petrogenesis. *Reviews in Mineralogy and Geochemistry*, *53*(1), 27–62. https://doi.org/10.2113/0530027

Hu, X., Garzanti, E., Moore, T., & Raffi, I. (2015). Direct stratigraphic dating of India-Asia collision onset at the Selandian (middle Paleocene, 59±1 Ma). *Geology*, *43*(10), 859–862. https://doi.org/10.1130/G36872.1

Hu, X., Garzanti, E., Wang, J., Huang, W., An, W., & Webb, A. (2016). The timing of India-Asia collision onset–Facts, theories, controversies. *Earth-Science Reviews*, *160*, 264–299. https://doi.org/10.1016/j.earscirev.2016.07.014

Hu, X., Wang, J., An, W., Garzanti, E., & Li, J. (2017). Constraining the timing of the India-Asia continental collision by the sedimentary record. *Science China Earth Sciences*, *60*(4), 603–625. https://doi.org/10.1007/s11430-016-9003-6

Hüsing, S. K., Zachariasse, W. J., Van Hinsbergen, D. J., Krijgsman, W., Inceöz, M., Harzhauser, M., et al. (2009). Oligocene–Miocene basin evolution in SE Anatolia, Turkey: Constraints on the closure of the eastern Tethys gateway. *Geological Society of London*, *311*(1), 107–132. https://doi.org/10.1144/SP311.4

Karaoğlan, F., Parlak, O., Hejl, E., Neubauer, F., & Kloetzli, U. (2016). The temporal evolution of the active margin along the Southeast Anatolian Orogenic Belt (SE Turkey): Evidence from U–Pb, Ar–Ar and fission track chronology. *Gondwana Research*, *33*, 190–208. https://doi.org/10.1016/j.gr.2015.12.011

Karaoğlan, F., Parlak, O., Klötzli, U., Thöni, M., & Koller, F. (2012). U–Pb and Sm–Nd geochronology of the ophiolites from the SE Turkey: Implications for the Neotethyan evolution. *Geodinamica Acta*, *25*(3–4), 146–161. https://doi.org/10.1080/09853111.2013.858948

Karaoğlan, F., Parlak, O., Klötzli, U. R. S., Thoeni, M., & Koller, F. (2013). U–Pb and Sm–Nd geochronology of the Kızıldağ (Hatay, Turkey) ophiolite: Implications for the timing and duration of suprasubduction zone type oceanic crust formation in the southern Neotethys. *Geological Magazine*, *150*(2), 283–299. https://doi.org/10.1017/S0016756812000477

Kaymakci, N., Inceöz, M., Ertepinar, P., & Koç, A. (2010). Late Cretaceous to recent kinematics of SE Anatolia (Turkey). In M. Sosson, N. Kaymakci, R. A. Stephenson, F. Bergerat, & V. Starostenko (eds). *Sedimentary Basin Tectonics from the Black Sea and Caucasus to the Arabian Platform* (Vol. 340(1), pp. 409–435). Geological Society, London, Special Publications. https://doi.org/10.1144/SP340.18

Keskin, M. (2003). Magma generation by slab steepening and breakoff beneath a subduction-accretion complex: An alternative model for collision-related volcanism in Eastern Anatolia, Turkey. *Geophysical Research Letters*, *30*(24). https://doi.org/10.1029/2003GL018019

Keskin, M., Pearce, J. A., & Mitchell, J. G. (1998). Volcano-stratigraphy and geochemistry of collision-related volcanism on the Erzurum–Kars Plateau, northeastern Turkey. *Journal of Volcanology and Geothermal Research*, *85*(1–4), 355–404. https://doi.org/10.1016/S0377-0273(98)00063-8

Khalatbari-Jafari, M., Juteau, T., Bellon, H., Whitechurch, H., Cotten, J., & Emami, H. (2004). New geological, geochronological and geochemical investigations on the Khoy ophiolites and related formations, NW Iran. *Journal of Asian Earth Sciences*, *23*(4), 507–535. https://doi.org/10.1016/j.jseaes.2003.07.005

Konak, N., Alan, İ., Bakırhan, B., Bedi, Y., Dönmez, M., Pehlivan, Ş., et al. (2015). Geological map of Turkey at 1:1 000 000 scale. Ankara Mineral Research and Exploration Institute (MTA) of Turkey.

Koshnaw, R. I., Schlunegger, F., & Stockli, D. F. (2021). Detrital zircon provenance record of the Zagros mountain building from the Neotethys obduction to the Arabia–Eurasia collision, NW Zagros fold–thrust belt, Kurdistan region of Iraq. *Solid Earth*, *12*(11), 2479–2501. https://doi.org/10.5194/se-12-2479-2021

Koshnaw, R. I., Stockli, D. F., & Schlunegger, F. (2019). Timing of the Arabia-Eurasia continental collision—Evidence from detrital zircon U-Pb geochronology of the Red Bed Series strata of the northwest Zagros hinterland, Kurdistan region of Iraq. *Geology*, *47*(1), 47–50. https://doi.org/10.1130/G45499.1

Kuşcu, İ., Tosdal, R. M., Gencalioğlu-Kuşcu, G., Friedman, R., & Ullrich, T. D. (2013). Late Cretaceous to middle Eocene magmatism and metallogeny of a portion of the southeastern Anatolian orogenic belt, east-central Turkey. *Economic Geology*, *108*(4), 641–666. https://doi.org/10.2113/econgeo.108.4.641

Lechmann, A., Burg, J. P., Ulmer, P., Mohammadi, A., Guillong, M., & Faridi, M. (2018). From Jurassic rifting to Cretaceous subduction in NW Iranian Azerbaijan: Geochronological and geochemical signals from granitoids. *Contributions to Mineralogy and Petrology*, *173*(12), 102. https://doi.org/10.1007/s00410-018-1532-8

Liu, Z., Zhu, D. C., Rezeau, H., Jagoutz, O., Wang, Q., & Eyuboglu, Y. (2022). Late Cretaceous transition from Calc-alkaline to alkaline magmatism in the eastern Anatolian Plateau: Implications for microblock collision timing. *Journal of Petrology*, *63*(12), egac119. https://doi.org/10.1093/petrology/egac119

Maffione, M., van Hinsbergen, D. J., de Gelder, G. I., van der Goes, F. C., & Morris, A. (2017). Kinematics of Late Cretaceous subduction initiation in the Neo-Tethys Ocean reconstructed from ophiolites of Turkey, Cyprus, and Syria. *Journal of Geophysical Research: Solid Earth*, *122*(5), 3953–3976. https://doi.org/10.1002/2016JB013821

Mazhari, S. A., Bea, F., Amini, S., Ghalamghash, J., Molina, J. F., Montero, P., et al. (2009). TKhoy he Eocene bimodal Piranshahr massif of the Sanandaj–Sirjan Zone, NW Iran: A marker of the end of the collision in the Zagros orogen. *Journal of the Geological Society*, *166*(1), 53–69. https://doi.org/10.1144/0016-76492008-022

McQuarrie, N., & van Hinsbergen, D. J. (2013). Retrodeforming the Arabia-Eurasia collision zone: Age of collision versus magnitude of continental subduction. *Geology*, *41*(3), 315–318. https://doi.org/10.1130/G33591.1

Meijers, M. J., Kaymakci, N., Van Hinsbergen, D. J., Langereis, C. G., Stephenson, R. A., & Hippolyte, J. C. (2010). Late Cretaceous to Paleocene oroclinal bending in the central Pontides (Turkey). *Tectonics*, *29*(4). https://doi.org/10.1029/2009TC002620

Meijers, M. J., Van Hinsbergen, D. J., Dekkers, M. J., Altıner, D., Kaymakci, N., & Langereis, C. G. (2011). Pervasive Palaeogene remagnetization of the central Taurides fold-and-thrust belt (southern Turkey) and implications for rotations in the Isparta Angle. *Geophysical Journal International*, *184*(3), 1090–1112. https://doi.org/10.1111/j.1365-246X.2010.04919.x

Metcalfe, I. (2013). Gondwana dispersion and Asian accretion: Tectonic and palaeogeographic evolution of eastern tethys. *Journal of Asian Earth Sciences*, *66*, 1–33. https://doi.org/10.1016/j.jseaes.2012.12.020

Miller, K. G., Browning, J. V., Schmelz, W. J., Kopp, R. E., Mountain, G. S., & Wright, J. D. (2020). Cenozoic sea-level and cryospheric evolution from deep-sea geochemical and continental margin records. *Science Advances*, *6*(20), eaaz1346. https://doi.org/10.1126/sciadv.aaz1346

Miyashiro, A. (1973). Paired and unpaired metamorphic belts. *Tectonophysics*, *17*(3), 241–254. https://doi.org/10.1016/0040-1951(73)90005-X

Moghadam, H. S., Corfu, F., Stern, R. J., & Lotfi Bakhsh, A. (2019). The Eastern Khoy metamorphic complex of NW Iran: A Jurassic ophiolite or continuation of the Sanandaj–Sirjan Zone? *Journal of the Geological Society*, *176*(3), 517–529. https://doi.org/10.1144/jgs2018-081

Moghadam, H. S., Li, Q. L., Stern, R. J., Griffin, W. L., & O'Reilly, S. Y. (2022). Zircon xenocrysts in Late Cretaceous magmatic rocks in the Kermanshah Ophiolite: Link to Iran continental crust supports the subduction initiation model. *International Geology Review*, *64*(22), 3248–3259. https://doi.org/10.1080/00206814.2022.2043193

Moghadam, H. S., & Stern, R. J. (2015). Ophiolites of Iran: Keys to understanding the tectonic evolution of SW Asia:(II) Mesozoic ophiolites. *Journal of Asian Earth Sciences*, *100*, 31–59. https://doi.org/10.1016/j.jseaes.2014.12.016

Mohamadi Chaghamarani, Z., Amel, N., Topuz, G., Moayyed, M., Koroneos, A., Köksal, S., & Küçük, A. (2025). Middle-to-Late Eocene shoshonitic basaltic volcanism in NW Iran (Kivi region): Implications for a buried Neo-Tethyan suture. *International Journal of Earth Sciences*, *114*(7–8), 1–23. https://doi.org/10.1007/s00531-025-02540-z

Montemagni, C., Zanchetta, S., Malaspina, N., Javadi, H. R., & Zanchi, A. (2023). The onset of Neo-Tethys subduction in the early Jurassic: Evidence from the eclogites of the North Shahrekord Metamorphic complex (Sanandaj-Sirjan Zone, W Iran). *Geological Magazine*, *160*(12), 2067–2090. https://doi.org/10.1017/S0016756824000098

Morris, A. (2003). The Late Cretaceous palaeolatitude of the Neotethyan spreading axis in the eastern Mediterranean region. *Tectonophysics*, *377*(1–2), 157–178. https://doi.org/10.1016/j.tecto.2003.08.016

Mouthereau, F., Lacombe, O., & Vergés, J. (2012). Building the Zagros collisional orogen: Timing, strain distribution and the dynamics of Arabia/Eurasia plate convergence. *Tectonophysics*, *532*, 27–60. https://doi.org/10.1016/j.tecto.2012.01.022

Nurlu, N., Parlak, O., Robertson, A., & Von Quadt, A. (2015). Implications of Late Cretaceous U–Pb zircon ages of granitic intrusions cutting ophiolitic and volcanogenic rocks for the assembly of the Tauride allochthon in SE Anatolia (Helete area, Kahramanmaraş Region, SE Turkey). *International Journal of Earth Sciences*, *105*(1), 283–314. https://doi.org/10.1007/s00531-015-1211-1

Oberhänsli, R., Bousquet, R., Candan, O., & Okay, A. I. (2012). Dating subduction events in east Anatolia, Turkey. *Turkish Journal of Earth Sciences*, *21*(1), 1–17. https://doi.org/10.3906/yer-1006-26

Oberhänsli, R., Candan, O., Bousquet, R., Rimmele, G., Okay, A., & Goff, J. (2010). Alpine high pressure evolution of the eastern Bitlis complex, SE Turkey. In M. Sosson, N. Kaymakci, R. A. Stephenson, F. Bergerat, & V. Starostenko (eds). *Sedimentary Basin Tectonics from the Black Sea and Caucasus to the Arabian Platform* (Vol. 40(1), pp. 461–483). Geological Society, London, Special Publications. https://doi.org/10.1144/SP340.20

Oberhänsli, R., Koralay, E., Candan, O., Pourteau, A., & Bousquet, R. (2013). Late Cretaceous eclogitic high-pressure relics in the Bitlis massif. *Geodinamica Acta*, *26*(3–4), 175–190. https://doi.org/10.1080/09853111.2013.858951

Okay, A. I., Arman, M. B., & Göncüoglu, M. C. (1985). Petrology and phase relations of the kyanite-eclogites from eastern Turkey. *Contributions to Mineralogy and Petrology*, *91*(2), 196–204. https://doi.org/10.1007/BF00377767

Okay, A. I., Sunal, G., Sherlock, S., Kylander-Clark, A. R., & Özcan, E. (2020). İzmir-Ankara suture as a Triassic to Cretaceous Plate Boundary—Data from central Anatolia. *Tectonics*, *39*(5), e2019TC005849. https://doi.org/10.1029/2019TC005849

Okay, A. I., Topuz, G., Kylander-Clark, A. R., Sherlock, S., & Zattin, M. (2022). Late Paleocene–Middle Eocene magmatic flare-up in western Anatolia. *Lithos*, *428*, 106816. https://doi.org/10.1016/j.lithos.2022.106816

Okay, A. I., & Tüysüz, O. (1999). Tethyan sutures of northern Turkey. In B. Durand, L. Jolivet, F. Horváth, & M. Séranne (eds). *The Mediterranean Basins: Tertiary Extension within the Alpine Orogen* (Vol. 156(1), 475–515). Geological Society of London Special Publications. https://doi.org/10.1144/GSL.SP.1999.156.01.22

Okay, A. I., Zattin, M., & Cavazza, W. (2010). Apatite fission-track data for the Miocene Arabia-Eurasia collision. *Geology*, *38*(1), 35–38. https://doi.org/10.1130/G30234.1

Okay, A. I., Zattin, M., Özcan, E., & Sunal, G. (2020b). Uplift of Anatolia. *Turkish Journal of Earth Sciences*, *29*(5), 696–713. https://doi.org/10.3906/yer-2003-10

Özcan, E., Less, G., Báldi-Beke, M., & Kollányi, K. (2010). *Oligocene hyaline larger Foraminifera from Kelereşdere section (Muş, Eastern Turkey)* (pp. 465–493). Micropaleontology. Retrieved from https://www.jstor.org/stable/40960130

Özdemir, Y., & Güleç, N. (2014). Geological and geochemical evolution of the Quaternary Süphan Stratovolcano, Eastern Anatolia, Turkey: Evidence for the lithosphere–asthenosphere interaction in post-collisional volcanism. *Journal of Petrology*, *55*(1), 37–62. https://doi.org/10.1093/petrology/egt060

Özer, S. (2025). Glabrobournonia Morris and Skelton (Rudist, Bivalvia) from the Campanian–Maastrichtian of Türkiye: Taxonomy, palaeoecology and palaeobiogeography. *Palaeoworld*, *34*(4), 100895. https://doi.org/10.1016/j.palwor.2024.11.003

Özgül, N., & Turşucu, A. (1984). Stratigraphy of the Mesozoic carbonate sequence of the Munzur Mountains (Eastern Taurides). In O. Tekeli & M. C. Göncüoğlu (Eds.), *Geology of the taurus Belt: Ankara, Turkey, Maden tetkit Arama Enstitüsü* (pp. 173–181).

Parlak, O. (2016). The tauride ophiolites of Anatolia (Turkey): A review. *Journal of Earth Science*, *27*(6), 901–934. https://doi.org/10.1007/s12583-016-0679-3

Pearce, J. A., Bender, J. F., De Long, S. E., Kidd, W. S. F., Low, P. J., Güner, Y., et al. (1990). Genesis of collision volcanism in Eastern Anatolia, Turkey. *Journal of Volcanology and Geothermal Research*, *44*(1–2), 189–229. https://doi.org/10.1016/0377-0273(90)90018-b

Perch-Nielsen, K. (1985). Cenozoic calcareous nannofossils. In H. M. Bolli, J. B. Saunders, & K. Perch-Nielsen (Eds.), *Plankton stratigraphy* (pp. 427–554). Cambridge University Press. https://doi.org/10.1016/0377-0273(90)90018-B

Perinçek, D., Duran, O., Bozdogan, N., & Çoruh, T. (1991). Stratigraphy and paleogeographical evolution of the autochthonous sedimentary rocks in Southeast Turkey. In S. Turgut (Ed.), *Tectonics and hydrocarbon potential of Anatolia and surrounding regions. Ozan Sungurlu Symposium, Proceedings of the Turkish Petroleum Corporation* (pp. 274–305). Turkish Association of Petroleum Geologists.

Pirouz, M., Avouac, J. P., Hassanzadeh, J., Kirschvink, J. L., & Bahroudi, A. (2017). Early Neogene foreland of the Zagros, implications for the initial closure of the Neo-Tethys and kinematics of crustal shortening. *Earth and Planetary Science Letters*, *477*, 168–182. https://doi.org/10.1016/j.epsl.2017.07.046

Premoli Silva, I., & Verga, D. (2004). *Practical manual of Cretaceous planktonic foraminifera: International school on planktonic Foraminifera*. Universities of Perugia and Milan.283.

Rabiee, A., Rossetti, F., Lucci, F., & Lustrino, M. (2022). Cenozoic porphyry and other hydrothermal ore deposits along the South Caucasus-West Iranian tectono-magmatic belt: A critical reappraisal of the controlling factors. *Lithos*, *430*, 106874. https://doi.org/10.1016/j.lithos.2022.106874

Reilinger, R., McClusky, S., Vernant, P., Lawrence, S., Ergintav, S., Cakmak, R., et al. (2006). GPS constraints on continental deformation in the Africa-Arabia-Eurasia continental collision zone and implications for the dynamics of plate interactions. *Journal of Geophysical Research*, *111*(B5). https://doi.org/10.1029/2005JB004051

Rızaoğlu, T., Parlak, O., Höck, V., Koller, F., Hames, W. E., & Billor, Z. (2009). Andean-type active margin formation in the eastern Taurides: Geochemical and geochronological evidence from the Baskil granitoid (Elazığ, SE Turkey). *Tectonophysics*, *473*(1–2), 188–207. https://doi.org/10.1016/j.tecto.2008.08.011

Rızaoğlu, T., Parlak, O., Hoeck, V., & İşler, F. (2006). Nature and significance of Late Cretaceous ophiolitic rocks and their relation to the Baskil granitic intrusions of the Elaziğ region, SE Turkey. In A. H. F. Robertson & D. Mountrakis (eds). *Tectonic Development of the Eastern Mediterranean Region* (Vol. 260(1), 327–350). Geological Society, London, Special Publications. https://doi.org/10.1144/gsl.sp.2006.260.01.14

Robertson, A., Boulton, S. J., Taslı, K., Yıldırım, N., İnan, N., Yıldız, A., & Parlak, O. (2016). Late Cretaceous–Miocene sedimentary development of the Arabian continental margin in SE Turkey (Adıyaman region): Implications for regional palaeogeography and the closure history of southern Neotethys. *Journal of Asian Earth Sciences*, *115*, 571–616. https://doi.org/10.1016/j.jseaes.2015.01k.025

Robertson, A. H., & Parlak, O. (2025). Eocene contractional deformation in the NW corner of the Arabian plate and its relation to Arabia-Eurasia collision in SE Türkiye. *International Geology Review*, *67*(6), 717–753. https://doi.org/10.1080/00206814.2024.2400696

Robertson, A. H., Parlak, O., & Ustaömer, T. (2012). Overview of the Palaeozoic–Neogene evolution of Neotethys in the Eastern Mediterranean region (southern Turkey, Cyprus, Syria). *Petroleum Geoscience*, *18*(4), 381–404. https://doi.org/10.1144/petgeo2011-091

Robertson, A. H., Ustaömer, T., Parlak, O., Ünlügenç, U. C., Taşlı, K., & Inan, N. (2006). The Berit transect of the Tauride thrust belt, S Turkey: Late cretaceous–early Cenozoic accretionary/collisional processes related to closure of the Southern Neotethys. *Journal of Asian Earth Sciences*, *27*(1), 108–145. https://doi.org/10.1016/j.jseaes.2005.02.004

Robertson, A. H. F., & Dixon, J. E. (1984). Introduction: Aspects of the geological evolution of the Eastern Mediterranean. *Geological Society*, *17*(1), 1–74. https://doi.org/10.1144/gsl.sp.1984.017.01.02

Robertson, A. H. F., Parlak, O., Ustaömer, T., Taslı, K., & Dumitrica, P. (2021). Late Palaeozoic-Neogene sedimentary and tectonic development of the Tauride continent and adjacent Tethyan ocean basins in eastern Turkey: New data and integrated interpretation. *Journal of Asian Earth Sciences*, *220*, 104859. https://doi.org/10.1016/j.jseaes.2021.104859

Rolland, Y., Hässig, M., Bosch, D., Bruguier, O., Melis, R., Galoyan, G., et al. (2020). The East Anatolia–Lesser Caucasus ophiolite: An exceptional case of large-scale obduction, synthesis of data and numerical modelling. *Geoscience Frontiers*, *11*(1), 83–108. https://doi.org/10.1016/j.gsf.2018.12.009

Rolland, Y., Perincek, D., Kaymakci, N., Sosson, M., Barrier, E., & Avagyan, A. (2012). Evidence for~ 80–75 Ma subduction jump during Anatolide–Tauride–Armenian block accretion and~ 48 Ma Arabia–Eurasia collision in Lesser Caucasus–East Anatolia. *Journal of Geodynamics*, *56*, 76–85. https://doi.org/10.1016/j.jog.2011.08.006

Rubatto, D. (2002). Zircon trace element geochemistry: Partitioning with garnet and the link between U–Pb ages and metamorphism. *Chemical Geology*, *184*(1–2), 123–138. https://doi.org/10.1016/S0009-2541(01)00355-2

Sar, A., Ertürk, M. A., & Rizeli, M. E. (2019). Genesis of Late Cretaceous intra-oceanic arc intrusions in the Pertek area of Tunceli Province, eastern Turkey, and implications for the geodynamic evolution of the southern Neo-Tethys: Results of zircon U–Pb geochronology and geochemical and Sr–Nd isotopic analyses. *Lithos*, *350*, 105263. https://doi.org/10.1016/j.lithos.2019.105263

Sarkarinejad, K., Godin, L., & Faghih, A. (2009). Kinematic vorticity flow analysis and 40Ar/39Ar geochronology related to inclined extrusion of the HP–LT metamorphic rocks along the Zagros accretionary prism, Iran. *Journal of Structural Geology*, *31*(7), 691–706. https://doi.org/10.1016/j.jsg.2009.04.003

Schaltegger, U., Zeilinger, G., Frank, M., & Burg, J. P. (2002). Multiple mantle sources during island arc magmatism: U–pb and Hf isotopic evidence from the Kohistan arc complex, Pakistan. *Terra Nova*, *14*(6), 461–468. https://doi.org/10.1046/j.1365-3121.2002.00432.x

Schleiffarth, W. K., Darin, M. H., Reid, M. R., & Umhoefer, P. J. (2018). Dynamics of episodic late Cretaceous–Cenozoic magmatism across Central to Eastern Anatolia: New insights from an extensive geochronology compilation. *Geosphere*, *14*(5), 1990–2008. https://doi.org/10.1130/GES01647.1

Schmitt, A. K., Konrad, K., Andrews, G. D., Horie, K., Brown, S. R., Koppers, A. A., et al. (2018). 40Ar/39Ar ages and zircon petrochronology for the rear arc of the izu-bonin-marianas intra-oceanic subduction zone. *International Geology Review*, *60*(8), 956–976. https://doi.org/10.1080/00206814.2017.1363675

Şengör, A. C., Özeren, M. S., Keskin, M., Sakınç, M., Özbakır, A. D., & Kayan, İ. (2008). Eastern Turkish high plateau as a small Turkic-type orogen: Implications for post-collisional crust-forming processes in Turkic-type orogens. *Earth-Science Reviews*, *90*(1–2), 1–48. https://doi.org/10.1016/j.earscirev.2008.05.002

Şengör, A. M. C. (1990). A new model for the late Palaeozoic Mesozoic tectonic evolution of Iran and implications for Oman. In A. H. F. Robertson, M. P. Searle, & A. C. Ries (eds.). *The Geology and Tectonics of the Oman Region* (Vol. 49(1), p. 797–831). Geological Society, London, Special Publication. https://doi.org/10.1144/GSL.SP.1992.049.01.49

Şengör, A. M. C. (1991). Plate tectonics and orogenic research after 25 years: Synopsis of a Tethyan perspective. *Tectonophysics*, *187*(1–3), 315–344. https://doi.org/10.1016/0040-1951(91)90427-T

Şengör, A. M. C., Özeren, S., Genç, T., & Zor, E. (2003). East Anatolian high plateau as a mantle-supported, north-south shortened domal structure. *Geophysical Research Letters*, *30*(24). https://doi.org/10.1029/2003GL017858

Şengör, A. M. C., & Yilmaz, Y. (1981). Tethyan evolution of Turkey: A plate tectonic approach. *Tectonophysics*, *75*(3–4), 181–241. https://doi.org/10.1016/0040-1951(81)90275-4

Sheikholeslami, M. R., Pique, A., Mobayen, P., Sabzehei, M., Bellon, H., & Emami, M. H. (2008). Tectono-metamorphic evolution of the Neyriz metamorphic complex, Quri-kor-e-sefid area (Sanandaj-Sirjan Zone, SW Iran). *Journal of Asian Earth Sciences*, *31*(4–6), 504–521. https://doi.org/10.1016/j.jseaes.2007.07.004

Şimşek, E., Parlak, O., Robertson, A., Çetinkaplan, M., Deniz, K., Aysal, N., et al. (2024). *Late Cretaceous upper amphibolite Facies metamorphism and tectonic setting of the pütürge massif (Malatya, Türkiye). 76th geological Congress of Türkiye. April 15-19, 2024, Ankara, Türkiye*. Abstract book p. 417.

Şimşek, E., Parlak, O., Robertson, A., Çetinkaplan, M., Yağcıoğlu, K. D., Aysal, N., et al. (2025). *Tectonic evolution of the pütürge metamorphites, Southeast Anatolia, Türkiye. 77th geological Congress of Türkiye Ankara, Türkiye. April 14-18, 2025. Ankara, Türkiye*. Abstract.

Stampfli, G. M., & Borel, G. D. (2002). A plate tectonic model for the Paleozoic and Mesozoic constrained by dynamic plate boundaries and restored synthetic oceanic isochrons. *Earth and Planetary Science Letters*, *196*(1–2), 17–33. https://doi.org/10.1016/S0012-821X(01)00588X

Stern, R. J., Moghadam, H. S., Pirouz, M., & Mooney, W. (2021). The geodynamic evolution of Iran. *Annual Review of Earth and Planetary Sciences*, *49*(1), 9–36. https://doi.org/10.1146/annurev-earth-071620-052109

Steuber, T., Özer, S., Schlüter, M., & Sarı, B. (2009). Description of Paracaprinula syriaca Piveteau (Hippuritoidea, Plagioptychidae) and a revised age of ophiolite obduction on the african-arabian Plate in southeastern Turkey. *Cretaceous Research*, *30*(1), 41–48. https://doi.org/10.1016/j.cretres.2008.04.001

Steuber, T., & Schlüter, M. (2012). Strontium-isotope stratigraphy of Upper Cretaceous rudist bivalves: Biozones, evolutionary patterns and sea-level change calibrated to numerical ages. *Earth-Science Reviews*, *114*(1–2), 42–60. https://doi.org/10.1016/j.earscirev.2012.04.004

Su, H., & Zhou, J. (2020). Timing of Arabia-Eurasia collision: Constraints from restoration of crustal-scale cross-sections. *Journal of Structural Geology*, *135*, 104041. https://doi.org/10.1016/j.jsg.2020.104041

Sun, G., Hu, X., Garzanti, E., BouDagher-Fadel, M. K., Xu, Y., Jiang, J., et al. (2023). Pre-Eocene Arabia-Eurasia collision: New constraints from the Zagros Mountains (Amiran Basin, Iran). *Geology*, *51*(10), 941–946. https://doi.org/10.1130/G51321.1

Tekin, U. K., Bedi, Y., Uzunçimen, S., Perincek, D., & Varol, E. (2011). Bajocian-Cenomanian pelagic sedimentation in the Koçalı Complex. SE Turley: Radiolarian datings. In *6th International Congress EMMM-2011, Russia*.

Topak, Y. (2022). The LA–ICP–MS Zircon U–Pb ages from the kuzgun Formation constrain the temporal distribution of the Adana Basin (Southern Turkey). *Geochemistry International*, *60*(13), 1439–1451. https://doi.org/10.1134/S0016702922130080

Topuz, G., Candan, O., Wang, J. M., Li, Q. L., Wu, F. Y., & Yılmaz, A. (2021). Silurian A-type metaquartz-syenite to-granite in the Eastern Anatolia: Implications for late Ordovician-Silurian rifting at the northern margin of Gondwana. *Gondwana Research*, *91*, 1–17. https://doi.org/10.1016/j.gr.2020.12.005

Topuz, G., Candan, O., Zack, T., Chen, F., & Li, Q. L. (2019). Origin and significance of early Miocene high-potassium I-type granite plutonism in the East Anatolian plateau (the Taşlıçay intrusion). *Lithos*, *348*, 105210. https://doi.org/10.1016/j.lithos.2019.105210

Topuz, G., Candan, O., Zack, T., & Yılmaz, A. (2017). East Anatolian plateau constructed over a continental basement: No evidence for the East Anatolian accretionary complex. *Geology*, *45*(9), 791–794. https://doi.org/10.1130/G39111.1

Topuz, G., Okay, A. I., Altherr, R., Schwarz, W. H., Siebel, W., Zack, T., et al. (2011). Post-collisional adakite-like magmatism in the Ağvanis Massif and implications for the evolution of the Eocene magmatism in the Eastern Pontides (NE Turkey). *Lithos*, *125*(1–2), 131–150. https://doi.org/10.1016/j.lithos.2011.02.003

Türkmen, I. (2004). Facies and evaporite genesis of the Kuşçular Formation (Lower Paleocene) saline playa complex, Eastern Turkey. *Journal of Asian Earth Sciences*, *24*(1), 91–104. https://doi.org/10.1016/j.jseaes.2003.09.007

Ural, M., Arslan, M., Göncüoglu, M. C., Tekin, K. U., & Kürüm, S. (2015). Late Cretaceous arc and back-arc formation within the Southern Neotethys: Whole-rock, trace element and Sr-Nd-Pb isotopic data from basaltic rocks of the Yüksekova Complex (Malatya-Elazığ, SE Turkey). *Ofioliti*, *40*(1), 57–72. https://doi.org/10.4454/ofioliti.v40i1.435

Ural, M., & Sari, M. K. (2019). Paleogeographic and Age findings on planktonic foraminiferal assemblages of Yuksekova complex in the Northeast of Elazig (Eastern Turkey). *Earth and Environmental Science*, *362*, 012146. https://doi.org/10.1088/1755-1315/362/1/012146

Ural, M., Sayit, K., Koralay, O. E., & Goncuoglu, M. C. (2021). Geochemistry and zircon U-Pb dates of felsic-intermediate members of the Late Cretaceous Yüksekova Arc Basin: Constraints on the evolution of the Bitlis–Zagros Branch of Neotethys (Elazığ, E Turkey). *Acta Geologica Sinica. English Edition*, *95*(4), 1199–1216. https://doi.org/10.1111/1755-6724.14694

Ural, M., Sayit, K., & Tekin, U. K. (2022). Whole-rock and Nd-Pb isotope geochemistry and radiolarian ages of the volcanics from the Yüksekova Complex (Maden area, Elazığ, E Turkey): Implications for a Late Cretaceous (Santonian-Campanian) back-arc basin in the southern Neotethys. *Ofioliti*, *47*(1), 65–83. https://doi.org/10.4454/ofioliti.v47i1.552

Ustaömer, P. A., Ustaömer, T., Collins, A. S., & Robertson, A. H. (2009). Cadomian (Ediacaran–Cambrian) arc magmatism in the Bitlis Massif, SE Turkey: Magmatism along the developing northern margin of Gondwana. *Tectonophysics*, *473*(1–2), 99–112. https://doi.org/10.1016/j.tecto.2008.06.010

Ustaömer, P. A., Ustaömer, T., Gerdes, A., Robertson, A. H., & Collins, A. S. (2012). Evidence of Precambrian sedimentation/magmatism and Cambrian metamorphism in the Bitlis Massif, SE Turkey utilising whole-rock geochemistry and U–Pb LA-ICP-MS zircon dating. *Gondwana Research*, *21*(4), 1001–1018. https://doi.org/10.1016/j.gr.2011.07.012

Uzuncimen, S., Tekin, U. K., Bedi, Y., Perincek, D., Varol, E., & Soycan, H. (2011). Discovery of the Late Triassic (Middle Carnian–Rhaetian) radiolarians in the volcano-sedimentary sequences of the Kocali Complex, SE Turkey: Correlation with the other Tauride units. *Journal of Asian Earth Sciences*, *40*(1), 180–200. https://doi.org/10.1016/j.jseaes.2010.08.004

van der Boon, A., Van Hinsbergen, D. J. J., Rezaeian, M., Gürer, D., Honarmand, M., Pastor-Galán, D., et al. (2018). Quantifying Arabia–Eurasia convergence accommodated in the Greater Caucasus by paleomagnetic reconstruction. *Earth and Planetary Science Letters*, *482*, 454–469. https://doi.org/10.1016/j.epsl.2017.11.025

van der Meer, D. G., Van Hinsbergen, D. J., & Spakman, W. (2018). Atlas of the underworld: Slab remnants in the mantle, their sinking history, and a new outlook on lower mantle viscosity. *Tectonophysics*, *723*, 309–448. https://doi.org/10.1016/j.tecto.2017.10.004

van Hinsbergen, D. J., Gürer, D., Koç, A., & Lom, N. (2024). Shortening and extrusion in the East Anatolian Plateau: How was Neogene Arabia-Eurasia convergence tectonically accommodated? *Earth and Planetary Science Letters*, *641*, 118827. https://doi.org/10.1016/j.epsl.2024.118827

van Hinsbergen, D. J. J., Torsvik, T. H., Schmid, S. M., Maţenco, L. C., Maffione, M., Vissers, R. L. M., et al. (2020). Orogenic architecture of the Mediterranean region and kinematic reconstruction of its tectonic evolution since the Triassic. *Gondwana Research*, *81*, 79–229. https://doi.org/10.1016/j.gr.2019.07.009

Varol, E., Bedi, Y., Tekin, U. K., & Uzuncimen, S. (2011). Geochemical and petrological characteristics of Late Triassic basic volcanic rocks from the Kocali complex; SE Turkey: Implications for the Triassic Evolution of Southern Tethys. *Ofioliti*, *36*(1), 101–115. https://doi.org/10.4454/ofioliti.v36i1.396

Verdel, C., Wernicke, B. P., Hassanzadeh, J., & Guest, B. (2011). A Paleogene extensional arc flare-up in Iran. *Tectonics*, *30*(3). https://doi.org/10.1029/2010TC002809

Vervoort, J. D., Plank, T., & Prytulak, J. (2011). The Hf–Nd isotopic composition of marine sediments. *Geochimica et Cosmochimica Acta*, *75*(20), 5903–5926. https://doi.org/10.1016/j.gca.2011.07.046

Wade, B. S., Pearson, P. N., Berggren, W. A., & Pälike, H. (2011). Review and revision of Cenozoic tropical planktonic foraminiferal biostratigraphy and calibration to the geomagnetic polarity and astronomical time scale. *Earth-Science Reviews*, *104*(1–3), 111–142. https://doi.org/10.1016/j.earscirev.2010.09.003

Wan, B., Chu, Y., Chen, L., Zhang, Z., Ao, S., & Talebian, M. (2023). When and why the NeoTethyan subduction initiated along the Eurasian margin: A case study from a Jurassic eclogite in southern Iran. *Compressional Tectonics: Plate Convergence to Mountain Building*, *1*, 245–260. https://doi.org/10.1002/9781119773856.ch9

Wang, C., Ding, L., Xiong, Z., Allen, M. B., Laskowski, A. K., Garzanti, E., et al. (2025). Timing of initial collision and suturing processes in the Himalaya and Zagros. *Nature Reviews Earth & Environment*, *6*(5), 357–376. https://doi.org/10.1038/s43017-025-00669-8

Yakymchuk, C., Kirkland, C. L., & Clark, C. (2018). Th/U ratios in metamorphic zircon. *Journal of Metamorphic Geology*, *36*(6), 715–737. https://doi.org/10.1111/jmg.12307

Yazgan, E. (1984). Geodynamic evolution of the Eastern Taurus region. In *Geology of the Taurus belt. International symposium* (pp. 199–208).

Yazgan, E., & Chessex, R. (1991). Geology and tectonic evolution of the southeastern Taurides in the region of Malatya. Turkish Association of Petroleum Geologists. *TPJD Bulletin*, *3*, 11–42.

Yılmaz, A., Topuz, G., Eken, T., Candan, O., & Yılmaz, H. (2023). Geology of the Eastern Anatolian Plateau (Turkey): A synthesis. *Turkish Journal of Earth Sciences*, *32*(4), 431–446. https://doi.org/10.55730/1300-0985.1854

Yılmaz, I. O., Cook, T. D., Hosgor, I., Wagreich, M., Rebman, K., & Murray, A. M. (2018). The upper Coniacian to upper Santonian drowned Arabian carbonate platform, the Mardin-Mazidag area, SE Turkey: Sedimentological, stratigraphic, and ichthyofaunal records. *Cretaceous Research*, *84*, 153–167. https://doi.org/10.1016/j.cretres.2017.09.012

Yılmaz, Y. (1993). New evidence and model on the evolution of the southeast Anatolian orogen. *Geological Society of America Bulletin*, *105*(2), 251–271. https://doi.org/10.1130/0016-7606(1993)105<0251:NEAMOT>2.3.CO;2

Yılmazer, S., Topuz, G., Guillong, M., Okay, A. I., Demirkaya, İ., & Uzun, F. (2025). Revealing the early geological history of the Istanbul Zone (Far-East Avalonia) through zircon U-Pb-Hf isotopic data. *Precambrian Research*, *427*, 107855. https://doi.org/10.1016/j.precamres.2025.107855

Yin, A. (2006). Cenozoic tectonic evolution of the Himalayan orogen as constrained by along-strike variation of structural geometry, exhumation history, and foreland sedimentation. *Earth-Science Reviews*, *76*(1–2), 1–131. https://doi.org/10.1016/j.earscirev.2005.05.004

Zarasvandi, A., Rezaei, M., Lentz, D., Pourkaseb, H., & Karevani, M. (2015). The Kasian volcanic rocks, Khorramabad, Iran: Evidence for a Jurassic intra-oceanic island arc in Neo-Tethys ocean. *Iranian Journal of Science and Technology*, *39*(A2), 165–178.

Zhang, Z., Xiao, W., Ji, W., Majidifard, M. R., Rezaeian, M., Talebian, M., et al. (2018). Geochemistry, zircon U-Pb and Hf isotope for granitoids, NW Sanandaj-Sirjan zone, Iran: Implications for Mesozoic-Cenozoic episodic magmatism during Neo-Tethyan lithospheric subduction. *Gondwana Research*, *62*, 227–245. https://doi.org/10.1016/j.gr.2018.04.002

Zhang, Z., Xiao, W., Majidifard, M. R., Zhu, R., Wan, B., Ao, S., et al. (2017). Detrital zircon provenance analysis in the Zagros Orogen, SW Iran: Implications for the amalgamation history of the Neo-Tethys. *International Journal of Earth Sciences*, *106*(4), 1223–1238. https://doi.org/10.1007/s00531-016-1314-3

Zor, E., Sandvol, E., Gürbüz, C., Türkelli, N., Seber, D., & Barazangi, M. (2003). The crustal structure of the East Anatolian plateau (Turkey) from receiver functions. *Geophysical Research Letters*, *30*(24). https://doi.org/10.1029/2003GL018192

Zuffa, G. G. (1985). Optical analyses of arenites: Influence of methodology on compositional results. In *Provenance of arenites* (pp. 165–189). Springer Netherlands.

10.1029/2025TC009243

References From the Supporting Information

Boynton, W. V. (1984). Geochemistry of rare Earth elements: Meteorite studies. In P. Henderson (Ed.), *Rare Earth element geochemistry* (pp. 63–114). Elsevier. https://doi.org/10.1016/B978-0-444-42148-7.50008-3

Berggren, W. A., Kent, D. V., Swisher III, C. C., & Aubry, M.-P. (1995). A revised Cenozoic geochronology and chronostratigraphy. In W. A. Berggren, D. V. Kent, M.-P. Aubry, & J. Hardenbol (Eds.), *Geochronology, time scales and global stratigraphic correlation* (Vol. 54, pp. 129–212). SEPM Special Publication.

Black, L. P., & Gulson, B. L. (1978). The age of the mud tank carbonatite, strange ways range, northern territory. *Journal of Australian Geology and Geophysics*, *3*, 227–232.

Coccioni, R., & Premoli Silva, I. (2015). Revised Upper Albian–Maastrichtian planktonic foraminiferal biostratigraphy and magnetostratigraphy of the classical Tethyan Gubbio section (Italy). *Newsletters on Stratigraphy*, *48*(1), 47–90. https://doi.org/10.1127/nos/2015/0055

Griffin, W. L., Powell, W. J., Pearson, N. J., & O'Reilly, S. Y. (2008). Appendix A2: Glitter: Data reduction software for Laser Ablation ICPMS. In P. Sylvester (Ed.), *Short course series 40. Laser ablation ICP–MS in the Earth sciences: Current practices and outstanding issues* (Vol. 40, pp. 308–311). Mineral Association of Canada.

Jackson, S. E., Pearson, N. J., Griffin, W. L., & Belousova, E. A. (2004). The application of laser ablation-inductively coupled plasma-mass spectrometry to in situ U–Pb zircon geochronology. *Chemical Geology*, *211*(1–2), 47–69. https://doi.org/10.1016/j.chemgeo.2004.06.017

Ludwig, K. R. (2012). *User's manual for Isoplot 3.75: A Geochronological Toolkit for Microsoft Excel* (Vol. 5, p. 75). Berkeley Geochronology Center Special Publication. Retrieved from https://www.geocalculate.com/wp-content/uploads/2019/10/Isoplot3_75-4_15manual.pdf

Martini, E. (1970). Standard Palaeogene calcareous nannoplankton zonation. *Nature*, *226*(5245), 560–561. https://doi.org/10.1038/226560a0

Martini, E. (1971). Standard Tertiary and Quaternary calcareous nannoplankton zonation. In A. Farinacci (Ed.), *Proceedings of the second planktonic conference* (Vol. 2, pp. 739–785). Edizioni Tecnoscienza.

Okada, H., & Bukry, D. (1980). Supplementary modification and introduction of code numbers to the low-latitude coccolith biostratigraphic zonation (Bukry, 1973, 1975). *Marine Micropaleontology*, *5*, 321–325. https://doi.org/10.1016/0377-8398(80)90016-X

Olsson, R. K., Berggren, W. A., Hemleben, C., & Huber, B. T. (1999). Atlas of Paleocene planktonic Foraminifera. *Smithsonian Contributions to Paleobiology*, *85*, 1–252.

Paton, C., Hellstrom, J., Paul, B., Woodhead, J., & Hergt, J. (2011). Iolite: Freeware for the visualisation and processing of mass spectrometric data. *Journal of Analytical Atomic Spectrometry*, *26*(12), 2508–2518. https://doi.org/10.1039/C1JA10172B

Paton, C., Woodhead, J. D., Hellstrom, J. C., Hergt, J. M., Greig, A., & Maas, R. (2010). Improved laser ablation U-Pb zircon geochronology through robust downhole fractionation correction. *Geochemistry, Geophysics, Geosystems*, *11*(3). https://doi.org/10.1029/2009GC002618

Sircombe, K. N. (2004). AgeDisplay: An EXCEL workbook to evaluate and display univariate geochronological data using binned frequency histograms and probability density distributions. *Computers & Geosciences*, *30*(1), 21–31. https://doi.org/10.1016/j.cageo.2003.09.006

Sissingh, W. (1977). Biostratigraphy of Cretaceous calcareous nannoplankton. *Geologie en Mijnbouw*, *56*, 37–65.

Thompson, J. M., Meffre, S., & Danyushevsky, L. (2018). Impact of air, laser pulse width and fluence on U–Pb dating of zircons by LA-ICPMS. *Journal of Analytical Atomic Spectrometry*, *33*(2), 221–230. https://doi.org/10.1039/C7JA00357A

Wu, F. Y., Yang, Y. H., Xie, L. W., Yang, J. H., & Xu, P. (2006). Hf isotopic compositions of the standard zircons and baddeleyites used in U-Pb geochronology. *Chemical Geology*, *234*(1–2), 105–126. https://doi.org/10.1016/j.chemgeo.2006.05.003